2D cell culture on soft hydrogel drives an endoplasmic reticulum stress-dependent S quiescence underlying molecular traits of pulmonary basal cells

Pierre-Alexandre Laval[1], Marie Piecyk[1], Paul Le Guen[1], Mirela Ilie[1], Joelle Fauvre[1], Isabelle Coste[1], Toufic Renno[1], Nicolas Aznar[1], Stephane Ansieau[1], Celine Hadji[4], Camille Migdal[4], Cedric Duret[1], Philippe Bertolino[1], Carole Ferraro-Peyret[1, 2], Alice Nicolas[3] and Cedric Chaveroux[1]*

Affiliations :

[1]Centre de Recherche en Cancérologie de Lyon, INSERM U1052, CNRS 5286, Centre Léon Bérard, Université de Lyon, Université Claude Bernard Lyon 1, Lyon, France.

[2] Hospices Civils de Lyon, Plateforme AURAGEN, Lyon, France.

[3]University Grenoble Alpes, CNRS, CEA/LETI Minatec, Grenoble Institute of Technology, Laboratory of Technology of Microelectronics, Grenoble, France.

[4]Cell&Soft, Grenoble, France.

Corresponding author:

*To whom correspondence should be addressed.

Email: cedric.chaveroux@lyon.unicancer.fr. Address: Cancer Research Center of Lyon, Inserm UMR 1052 CNRS 5286, Cheney D, floor 6, Centre Léon Bérard, 28 rue Laënnec, 69008 LYON, France. Tel: +33 (0)4 69 16 66 22

Keywords: Uniform soft hydrogel, S-phase quiescence, cell drift and differentiation capability, physiological ER stress, resistance to metabolic stress.

Summary

By preserving progenitor characteristics, cell culture on soft hydrogel represents a practical tool in regenerative medicine compared with conventional rigid plastic. However, the mechanism by which the mechanical microenvironment determines progenitor phenotype, and its relevance to human biology, remain poorly described. Thanks to an innovation enabling the generation of uniform multi-well hydrogels, we show that 2D culture on mechanomimetic supports leads to an atypical S-phase quiescence and prevents cell drift, while preserving the differentiation capacities of human bronchoepithelial cells. Mechanistically, defects in proteostasis and basal endoplasmic reticulum stress (ERS) underlie the quiescent phenotype and resistance to ERS-induced apoptosis by metabolic stress. Furthermore, analysis of available single cell data of the human lung confirmed that these molecular features are consistent with those of pulmonary basal cells. Overall, this study demonstrates that mechanomimetic supports are relevant devices for characterizing novel molecular events that govern progenitor biology in human tissues.

Introduction

As cells sense the extracellular mechanics, the interest for extracellular forces on cell behavior and fate importantly increased during the recent years. The mechanical signals directly influence the cell identity and subsequently their response to extracellular cues including therapeutic and microenvironmental stresses [1,2]. By extension, the relevance of regular tissue culture plastic (TCP) has been questioned as this matter displays an extraphysiological rigidity (in the range of gigapascal) that promotes abnormal cell polarization and loss of differentiation potential [3,4]. Furthermore, prolonged culture on TCP is associated with cell drift along passages, a well-known issue underlying reproducibility crisis[5]. In contrast, hydrogel coated plates represent a biocompatible support able to reproduce the mechanical properties of the tissue of interest. These 2D supports, whose compliance is close to that encountered by cells *in vivo,* are similar in use to regular TCP [6]. The possibility to amplify cells at large scale and its compatibility with commercially available cell live imagers pave the way of the use of hydrogel coated plates a practical and relevant alternative to 3D models, notably for high throughput screening. Still, the utilization and acceptance by the community of soft supports as a relevant alternative to TCP necessitates to: i) provide a robust protocol of support generation to ensure data reliability and ii) validate that the biology of the cells grown on soft matrix mirrors the one in human tissues.

Indeed, the fabrication of plates with soft bottoms is far from standard and although efforts have been put in the last 15 years to design soft bottom multi-well plates, critical issues remain. Two main difficulties are identified: i) the need to have a reduced variability of the mechanical properties and the surface chemistry in between wells, while ii) ensuring no fluids leakage and exchange between wells. Several developments tried to fix these issues including polymerization of the hydrogel well per well or the fabrication of hydrogel spots to be enclosed by a multiwell frame [7,8]. While the first strategy makes it difficult to control: i) the flatness, ii) the interwell reproducibility, iii) the absence of unpolymerized toxic residues and iv) the thickness of the hydrogel layer[8] the second strategy meets the difficulty of sealing the engineered bottom to the upper frame. For the latter, controlling the absence of interwell leaks is critical and at the moment, the proposed solution of clamping the both parts at the edges of the plates does not provide robust mitigation due to the deformability of the upper frame [9].

These technological issues contribute to the overall poorly addressed question consisting in determining whether tissue culture on soft supports is a relevant model reflecting the cell biology in human. Indeed, while there is an extensive literature documenting the differences between cellular responses on 2D soft substrates and TCP (for review [10]), it remains to be assessed whether cells grown on mechanomimetic supports not only behave differently from those grown on TCP but also retain better physiological characteristics. In terms of phenotypical impact, a large number of studies report that culture on biomimetic hydrogels represses cell

proliferation and favors a quiescent phenotype associated to the maintenance of pluripotency in numerous models compared to standard conditions of culture at early passages [11,12]. Pluripotent epithelial cells possess the ability to differentiate into a specific cell type upon specific cues. Consistently, in adult tissue, the number of proliferative cells are rare indicating that the majority of the cells reside as quiescent or senescent state to preserve their functional features [13]. Loss of quiescence leads to stem cell depletion and defect in tissue regenerative capacities illustrating the tight connection between cell identity and proliferative state. However, the term “quiescence” is widely used for designating a reversible non-proliferative state enabling cells to reenter the cell cycle [14]. Although often restricted to exiting the G1 phase towards G0, numerous type of quiescent states have been described along the cell cycle [15–17]. Few reports suggest that mechanical cues halt cells but not in G0 phase, suggesting that an atypical quiescence might underlie progenitor states in cells grown on hydrogel-based supports [18,19]. Furthermore, the fundamental mechanisms by which hydrogel supports trigger quiescence is still unknown. Cell quiescence is classically triggered following microenvironmental cues, including nutritional deprivation. This functional analogy between cells subjected to metabolic stress or grown on soft matrix suggests that common pathway(s) related to nutrient sensors might be involved in the mechanical-driven modification of cell fate. The endoplasmic reticulum (ER) is considered as a nutrient sensing organelle [20]. Upon nutritional stresses, the subsequent accumulation of misfolded proteins within the ER lumen leads the ER stress (ERS) and activation of the relative signaling pathways called unfolded protein response (UPR). The UPR then orchestrates of a complex transcriptional, posttranscriptional and translational reprogramming contributing to the restoration of cellular homeostasis and plasticity. Nonetheless, the ERS molecular axes are now emerging as key molecular events also implicated in the sensing of mechanical cues and cell identity changes [21]. Whether cells grown on hydrogels display proteostasis defects, dysregulated ERS signaling that might support cell cycle arrest and phenotypic modifications remains unknown.

Therefore, in this present study, we introduce a novel methodology for the generation of multiwell plate hydrogels drastically improving the interwell homogeneity and reliability of the desired stiffness compared to the classical method. Based on this innovation, we aimed at: i) defining whether slow proliferative capacities on mechanomimetics hydrogels are associated with the acquisition of a specific type of quiescence and/or senescence, ii) determining whether 2D soft supports enable long lasting cell culture with a reduced cell drift, and iii) whether this phenotype is controlled by a chronic ER stress. Taking human bronchoepithelial cells (HBEC-3KT) as a model of pulmonary cells, we show that cell culture on hydrogel plates favors a quiescent state in S phase preserving differentiation capabilities along passages., We also demonstrate that Ca^{2+} depletion in the ER, subsequent chronic proteostasic and phosphorylation of eIF2a drive this non-canonical

quiescence state. Finally, we show that this observation is consistent with the biology of pulmonary basal cells in human lung and render cells resistant to exogenous lethal metabolic stress. Our interdisciplinary study validates the use of soft supports as relevant culture tools for investigating the progenitor biology and unveils the UPR as novel molecular mechanisms at the interface of mechanical cues and cell identity decision in pulmonary basal cells.

Results

Development of a new methodology for improving stiffness reliability in multiwell plate hydrogels

Reliable and comparable evaluation of the biological substratum governing cellular dynamics within hydrogels hosted in multiwell plates mandates uniform stiffness prevailing across distinct well compartments within a given plate. As described above, the current limitations implicated the development of a new strategy to ensure softness homogeneity across the different wells of the plate. Inspired from the work of Ahmed et al, engineering soft supports in the 6-well plate was prioritized. This format not only serves as a convenient platform for real-time imaging but also furnishes ample biological matter to facilitate subsequent biochemical and molecular analyses [9]. First a polyacrylamide hydrogel layer was uniformly UV-cured on a multiwell-sized plate glass base treated to allow the covalent binding of the hydrogel. Before UV-exposure, the prepolymer solution was covered by a transparent hydrophobic glass slide equipped with 40 µm high wedges (Figure 1A). Thus, the polymerized hydrogel had a flat surface and exhibited a constant thickness throughout. Tuning the exposure time allowed to tune the stiffness of the hydrogel. Extensive rinsing could be performed to remove unreacted compounds [9]. In contrast to the clamping method, the hydrogel layer was sealed to the bottomless multi-well frame using a non-toxic liquid adhesive (Figure 1B). The glue was penetrating in the depth of the hydrogel thus guaranteeing a water-tight barrier in between the wells. To address the impact of soft matrix on pulmonary cell biology, 6-well plates were generated with 3 kPa polyacrylamide bottoms that is in the range of physiological pulmonary rigidities found in human samples [22,23]. Atomic force microscopy measurements confirmed that this technology enabled a high degree of uniformity within every well and in between the wells of the stiffness measured at 3.3+/-0.5 kPa (noted 3 kPa hereafter for the sake of simplicity) (Figure 1C). Furthermore, as polyacrylamide is not permissive to cell adhesion, the surface of the hydrogel was then coated well per well with collagen I (1 µg/cm^2), a major component of the lung matrisome [24]. The uniformity of matrix coating was achieved by evaporating the protein solution until the hydrogel surface was dried and confirmed by immunofluorescence (Figure 1D). TCP wells were also coated with the same matrix for establish the phenotypic contribution of the substrate stiffness only without introducing any bias through the biochemical environment. Since the starting material is a large hydrogel instead of polymerizing the hydrogel well per well, this novel approach can be extended to smaller multiwell soft supports and offers the possibility to fabricate a large amount of plates at once without apparent interwell leakage (Supplementary figure 1A, B).

Pulmonary mechanomimetic 2D supports promote an atypical quiescence in S phase

To investigate the impact of mechanomimetic hydrogels on lung cell identity at early and late passages, human broncho-epithelial cells (HBEC-3KT) were seeded on regular TCP dishes or on flat 3 kPa polyacrylamide

hydrogels (Figure 2A). Confluency measurement confirmed the compatibility of our innovation with classical live-imager similarly to TCP supports and revealed that cells grown on soft supports were proliferating much slower than those evolving on TCP (Figure 2B, C). We found that less than 10% of cells were stained for the proliferation marker KI67 on soft supports compared to 60% on TCP (Figure 2D). The number of KI67-positive cells found on 3 kPa were closely similar to the number of KI67-positive epithelial cells as previously described in the human normal lung (11.3 %) suggesting that cell culture on a 3 kPa soft substrate mimics better the pulmonary physiology [25]. In addition, cells remained active since the mobility was not affected by the soft hydrogel compared to regular plastic support (Figure 2E). To determine whether this slow-proliferating phenotype is maintained in long-term culture, HBEC-3KT were maintained either on TCP or 3 kPa supports for 20 passages and the doubling time was determined every 5 passages (Figure 2F). Although the doubling time of these cells was about 2 days on plastic, it drastically increased up to about 7 days once the cells were maintained on 3 kPa supports. In both cases, this index remained fairly stable over time, regardless the stiffness of the supports.

Slow/non-proliferating cells are often qualified as quiescent or senescent depending on their capabilities to progress again in the cell cycle once put back in proliferative conditions. Non-proliferating cells phenotypically often display cellular enlargement [26]. Consistently, HBEC-3KT cells grown on 3 kPa showed a significant increase of cell area and this phenotype was conserved even after 20 cell passages (Figure 3A). Gene expression analysis of common canonical markers of quiescence and senescence (*P16*, *P21*, *P27* and *FOXO3A*) confirmed the change of cell state (Figure 3B). To determine whether these changes are associated to a higher degree of senescence, a ß-galactosidase assay was performed (Figure3C). We observed that cell culture on the soft matrix increased significantly the number of senescent cells compared to TCP. Nevertheless, this fraction represented only 12% of the total population indicating that, on soft substrate, the majority of HBEC-3KT cells were blocked in a quiescent state. The precise localization of quiescent HBEC-3KT within the cell cycle was analyzed by flow cytometry. Figure 3D shows that HBEC-3KT grown on soft supports halted in S phase whereas we observed a drastic drop of cells localized in the G0/G1 phase compared to the TCP condition. However, no difference was found between the two conditions regarding the proportion of cells in G2/M phase. These experiments illustrate that HBEC-3KT grown on soft supports display an atypical quiescent state in S phase instead of the canonical G0 arrest. To assess whether these cells maintain their capacity to re-enter into a proliferative state, the cells were grown one passage on TCP or 3 kPa supports, then cross-seeded either on 3 kPa or on TCP supports and the confluency index was measured (Figure 3E). As expected, a severe repression of proliferation was observed when the cells were grown on 3 kPa supports independently

of the support of origin. However, when cells grown on soft hydrogel were transferred to TCP, they regained in large part their proliferative capacity.

Human bronchoepithelial cells grown on 2D soft supports show limited phenotypical drift after 20 passages

Similarly to our *in-vitro* observations, progenitor cells reside in a quiescent state in the adult normal tissue [27,28]. Thus, we sought to determine whether growing HBEC-3KT on soft matrix preserves their capacity to differentiate. This cell line has the capability to form alveoli once the cells are transferred on air-liquid interface (ALI) system. Thus, we tested whether the support rigidity and its associated cell identity changes the HBEC-3KT capacity of alveogenesis (Figure 4A). Interestingly, when the cells are grown on an ALI membrane, which is a stiff porous membrane, the increased cell area caused by the soft support is maintained regardless the number of passages, indicating that growing cells on the rigid ALI membrane does not reverse this phenotype (Figure 4B). However, we noticed that, for both conditions, cell area at late passage (P20) was lower than at the early passage (P2), which could suggest that cells underwent a phenotypic drift in both culture conditions. At P20, soft supports still exhibited significantly larger cells than the TCP counterparts. We then evaluated their phenotype drift by analyzing the evolution of their differentiation potential along passages. This was first done by measuring the expression of classical markers of pulmonary progenitors (*KRT5*, *KRT14* and *TP63*) (Figure 4C). At P2, the expression level of these genes was not significantly different between the two types of supports. However, at P20, this was significantly reduced for cells grown on TCP whereas it was maintained in cells grown on 3 kPa supports. This indicates that cell culture on 3 kPa maintains the HBEC-3KT pool of progenitors and differentiation potential. Then, a differentiation protocol was conducted. After 21 days, the ALI membranes were harvested and histological assessment of alveoli formation was performed (Figure 4D). Consistent with the gene expression assays, we did not observe a significant change in the ability of HBEC-3KT cells to generate alveoli at P2. However, at P20, the cells beforehand grown on TCP failed to generate alveoli whereas this ability was maintained for the cells previously grown on 3 kPa. At the transcriptional level, although the expression ratio of the alveolar markers (*PDPN* and *ACE2*) was not different in the differentiated tissues from P2, this was strongly increased in differentiated alveolar tissue from cells grown on soft compared to TCP at P20 (Figure 4E)

Overall these data demonstrate that mechanomimetic substrates promotes the acquisition of a quiescent phenotype in S phase. This non-canonical type of quiescence is associated to the preservation of progenitor pool and differentiation capabilities of pulmonary cells along passages.

Cells grown on soft supports display alteration of protein synthesis but not DNA damages

Then we sought to identify the mechanisms limiting the S/G2 transition. Although several molecular and metabolic pathways are implicated in the maintenance of a G0 quiescent state, those supporting this atypical state of quiescence are poorly described. Activation of the DNA damage response (DDR) and particularly the ATR signaling pathway constitute a cell cycle checkpoint regulating the S/G2 transition [29]. The ATR signaling pathway is classically activated by DNA replication stress leading to the phosphorylation of Chk1. However the ATM-KAP1 axis has been suggested to also being activated upon replication stress induced by a metabolic stress [30]. To determine whether induction of the DDR pathways impairs the S/G2 transition, canonical markers of both axes have been assessed by western blot (Figure 5A). Although, phosphorylation of ATM, KAP1 and Chk1 was expectedly increased in HBEC-3KT cells treated with the DNA damaging agent etoposide, cells grown on TCP or 3 kPa did not show marks of an activated DDR at basal states [31]. Thus, a role for the DDR activation in the accumulation of HBEC-3KT cells in S phase was excluded.

To obtain insight into the major pathways dysregulated on 3 kPa compared to TCP, RNA extracts from cells grown in both conditions were subjected to sequencing analysis at P2 and P20 (Figure 5B). At P2, we observed a large number of genes whose expression is dysregulated by the soft matrix (Figure 5C). Gene enrichment analysis unveiled a downregulation of factors associated to translation initiation pathway when the cells are grown on 3 kPa, suggesting an alteration of the protein synthesis process (Figure 5D-F). Similar results were obtained at P20 (Supplementary figure 2A, B). To functionally validate this translational impairment on soft substrate, a puromycin incorporation assay was performed on cells grown on both supports (Figure 5G). Western blot analysis revealed a lower incorporation of this antibiotic in elongating peptide demonstrating a decreased protein synthesis rate in cells grown on 3 kPa supports.

Cells grown on soft supports exhibit an endoplasmic reticulum calcium leakage and activated ER stress at steady state

Since the RNA-sequencing data oriented towards a defect of the initiation step of translation, we next explored the underlying molecular pathway. The phosphorylation of eIF2a (p-eIF2a) is known to: i) limit the initiation step of translation and ii) favors a specific translational program, including the elevation of the amount of the transcription factor ATF4, both driving cell plasticity upon microenvironmental cues [32]. Furthermore, the phosphorylation of eIF2a is reported to trigger a cell cycle arrest in G1/S or G2/M upon chemical stressors [33,34]. We therefore investigated whether activation of this pathway could contribute to cell quiescence in S phase observed on soft supports. Western blotting analysis revealed an augmentation of p-eIF2a and ATF4 in cells grown on 3 kPa compared to TCP (Figure 6A). These elevations are accompanied by an increase of BiP,

a chaperone whose augmentation is a canonical marker of an activated ERS signaling. Furthermore, the expression of canonical ERS markers (*ASNS*, *TRIB3*, *CHOP* and *P58IPK)* was increased in cells grown on soft substrates compared to TCP (Figure 6B). Furthermore, since ERS results from an impairment of protein homeostasis, the presence of aggresomes in cells grown on the soft supports was investigated (Figure 6C). Ubiquitin-positive foci attested the occurrence of protein aggregates in these cells. Altogether, these results confirm cells grown on 3 kPa exhibit proteostasis defects and an active ERS at basal level.

Then, we investigated the causality of the chronic ERS in cells grown on soft supports. Accumulation of protein aggregates classically results from either an impairment of the hexosamine biosynthetic pathway (HBP) and subsequent inhibition of protein N-glycosylation or a leakage of Ca^{2+} impairing the ER-chaperones folding activity [35,36]. We first tested whether a metabolic stress and subsequent glycosylation defects might be involved. To this end, the glycosylation of CD98, an adaptor of amino acid transporter and a model protein for assessing N-glycosylation process, was evaluated by Western blotting (Figure 6D) [37]. Although glucose deprivation on TCP, impairing the HBP, consistently diminished the CD98 N-glycosylation as revealed by the appearance of a lower band, we did not observe such hypoglycosylated form of CD98 in cells grown on the 3 kPa supports, thus leading to the conclusion that the chronic ERS is not caused by a defect in glycosylation. Additionally, gene expression analysis of the ERS canonical target genes was performed after medium renewal in order to exclude any nutrient exhaustion that may have triggered the UPR (Figure 6E). The expression degree of these markers remained higher in cells grown on soft substrates compared to TCP support Collectively, these results indicate that the ERS observed in cells grown on soft supports does not result from an alteration of the metabolic microenvironment. As mentioned above, the ERS can also be triggered through the impairment of the Ca^{2+} homeostasis within this organelle. Then we tested whether cells grown on 3 kPa supports display a defects of Ca^{2+} storage within the ER. To this end, a chemical reporter was used for visualizing the free intracellular Ca^{2+}. Validation experiment combining this chemical with an ER tracker confirmed that this ion is majorly localized in the ER lumen at basal state in the HBEC-3KT grown on TCP (Supplementary figure 3). Then assessment of intracellular Ca^{2+} concentrations revealed a lower accumulation of Ca^{2+} in cells grown on 3 kPa compared to TCP providing a causal explanation to the chronic ERS observed on soft supports (Figure 6F).

The eIF2a branch drives the S-phase quiescence and soft matrix confers protection to ERS-mediated cell death by metabolic stress.

Beyond its classical role of translation modulator, we then sought to establish whether the phosphorylation of eIF2a could be a cell cycle checkpoint controlling the S/G2 transition. To this end, cells grown on 3 kPa were

treated with ISRIB, a compound impairing the eIF2a phosphorylation [39]. ISRIB expectedly reduced the expression of ATF4 target genes (Figure 7A). At the contrary the mRNA level of P58IPK, whose expression is driven by the IRE1-XBP1 branch of the ERS, was not affected confirming ISRIB efficacy and selectivity[40]. Furthermore, the expression level of quiescence genes was also decreased to a degree closed to HBEC-3KT grown on TCP, indicating that p-eIF2a is driving the induction of quiescence markers in cells grown on soft supports. To determine the contribution of p-eIF2a in the cell cycle halt in S phase, cells grown on the soft substrates and treated or not with ISRIB and the consequences on the cell cycle were analyzed by flow cytometry (Figure 7B). ISRIB promotes the cell cycle progression as it significantly lowers the accumulation of cells in the S-phase and we observed a trend of increased proportions of HBEC-3KT in G2/M and G0/G1 phases. These data demonstrate that alleviating the eIF2a phosphorylation permits the bypass of the S-phase quiescence in cells cultivated on soft supports.

Finally, we intended to determine whether a chronic ERS could interfere with the cellular outcome upon microenvironmental cues and particularly glucose shortage. Lack of glucose is found in various diseases including cancer, ischemia-reperfusion or neurodegenerative diseases [41–43]. Upon irremediable hypoglycemic stress, ATF4 orchestrates the cell death by directly inducing the expression of proapoptotic genes including *CHOP, TRIB3* and *cFOS* [44,45]. However it has been shown that prior activation of the ERS and subsequent feedbacks involving P58IPK inhibit the p-eIF2a signaling and prevent cells from the ATF4-mediated apoptosis upon ER stressors [46,47]. Thus, as a functional validation of the basal proteostasic stress occurring in cells grown on soft supports, we hypothesized that culture on pulmonary mechanomimetic supports might confer resistance to exogenous lethal ERS, including glucose starvation (Figure 7C). To avoid any bias caused by differential glucose uptake and metabolism according to the tested rigidities, cells grown on 3 kPa or TCP were subjected to complete glucose starvation [48]. As expected, we did not measured any dead cells at basal between TCP and 3kPa whereas an important cell death was measured in cells grown on TCP subjected to glucose starvation. However this loss of viability was completely abrogated on soft supports demonstrating that this matrix and the subsequent molecular rewiring protects the cells from a lethal metabolically-induced ER stress. Consistently, transactivation by glucose deprivation of ATF4-proapoptotic target genes, including CHOP, was much lower in cells grown on 3 kPa compared to TCP (Figure 7D). Overall these data demonstrate that the ERS signaling, particularly the eIF2a branch, drives the phenotypic changes of cells grown on soft matrix.

2D mechanomimetic substrates maintain proteostasis dysfunction like that of human pulmonary basal cells

Overall, our data revealed that epithelial lung cells grown on 3 kPa polyacrylamide hydrogels coated with collagen I display profound molecular and biochemical reprogramming underlying cell state changes towards a basal identity. Defining whether these characteristics are artefactual or come under progenitor biology is crucial for validating the relevance of our findings in human and, in general the capacity of 2D mechanomimetics supports to mimic the *in vivo*. Therefore, we first sought to identify the pathways specifically dysregulated in basal cells in the human pulmonary tissue. To this end, publicly available data from single cells experiments performed on human lungs were interrogated and gene ontology analyses were performed on the previously identified genes characterizing the different cell clusters of the airway (Figure 8A) [49]. Our results confirmed that the major dysregulated processes in basal cells are closely related to translation and proteostasis reinforcing the translational characteristics of this cellular subpopulation. Then, we assessed whether an active ERS signaling is found specifically in these cells. To this end, we compared in the non-secretory contingency of epithelial cells the enrichment of the gene signature related to the UPR (Figure 8B). Consistently, basal cells show a higher enrichment for the UPR signature compared to the differentiating basal and ciliated cells indicating that the UPR is a molecular determinant of the progenitor identity in the lung. Overall, these data validate the *in vitro* data in the human lung tissue and confirm the relevance of mechanomimetic hydrogels to closely reproduce the progenitor biology for preclinical studies.

Discussion

The use of mechanomimetic supports for cell culture has gained an important interest for the last twenty years because of the development of mechanobiology and advances in understanding how the physical properties of tissues drive cell behavior or pathology development [10]. Consistently, this technology has been transferred to refine drug screening, disease modeling or tissue regeneration. Nonetheless, technological issues regarding their fabrication and the underlying molecular mechanism supporting the progenitor identity and mostly the relevance of the cell biology towards the original tissue were still unclear.

Herein we introduce an innovation oriented toward the design of soft bottom, multiwell plates solving the issues associated to stiffness heterogeneity across wells while ensuring impermeability of the wells. This development has facilitated the systematic examination of cellular proliferation over a span of 20 passages and allowed to conduct in parallel live imaging and biochemical and molecular analyses such as Western Blot, qPCR and RNA sequencing. At the biological level, although the impact of hydrogels on cell proliferation has been extensively reported [50], the type of quiescence induced by such supports remained unclear. In this study, we demonstrate that mechanomimetic supports triggers a drastic decreased of the S/G2 transition and an atypical quiescent state in S phase but not in the canonical G0. This state remains associated with the preservation of the progenitor capabilities of the basal cells and differentiation capabilities along passages. Whether hydrogel-driven accumulation of lung progenitor cells in S phase is representative of the *in vivo* physiology remains determinant for the validation of such supports in biology or as a relevant alternative to animals' usage in preclinical studies. Incorporation of BrdU allows the detection of cells with active DNA replication and thus localized in S phase [51]. In lungs of mice and pork, the latter being proposed as a closer model to human tissue, the large majority of pulmonary basal/stem cells are positive for BrdU whereas other epithelial cells show a very poor proportion of BrdU incorporation [52,53]. These data thus show that the positioning in the cell cycle of lung cells grown on 2D mechano-mimetic supports closely mimics the biology of progenitors *in vivo*, where these cells are positioned in the S phase. The S phase ensures DNA replication and the transition towards the G2 phase. Maintenance of the genome integrity is critical in dividing cells, especially progenitors and, consistently, the S/G2 checkpoint is notably controlled by the ATR kinase sensing stressed replication forks [29]. Nonetheless, since we did not observe an elevation of molecular markers related to DNA damages and the ATR signaling pathway, we conclude that cell accumulation in S phase does not result from alterations within the DNA. This latter is critical since amplification at large scale of cell progenitors, including the mesenchymal stem cells, without damaging the DNA is a key challenge for regenerative medicine and cellular therapy [54]. Instead of a contribution of the DDR pathways, we propose that the phosphorylation of eIF2a actively contributes to the maintenance of the S-quiescence. The role of this molecular event on the cell cycle,

particularly in progenitors, remains unclear. P-eIF2a has been proposed as a checkpoint for the G1/S or G2/M transition [33,34]. In these previous studies, the contribution of p-eIF2a to the cell cycle arrest was investigated by using chemicals that might have pleiotropic effects and can artificially influence the phase in which the cell is arrested. At the contrary, in this study, the underlying signal inducing p-eIF2a is generated by the non-genotoxic physiological mechanics, as attested by absence of DDR activation. This indicates that the role of the eIF2a phosphorylation on the cell cycle arrest might be context dependent but is rather associated to a prolonged S phase in cycling cells upon physiological conditions. The relevance of a constitutively phosphorylated form of eIF2a in the normal physiology of cell progenitors is attested in several tissues. Indeed, p-eIF2a is abundant and promotes pluripotency of mouse and human embryonic stem cells [55]. Furthermore activation of the ER stress signaling is essential for the reprogramming of somatic cells into induced pluripotent stem cells (IPSCs) [56]. In line with these assumptions, p-eIF2a is implicated in the conservation of the stemness of hematopoietic cells and the maintenance of stem cell quiescence and self-renewal in the muscle of mice [57,58]. This specific subpopulation of cells are characterized by a prolonged S-phase of 14 hours and thus are not blocked in G0/G1, demonstrating that indeed, physiological ERS and p-eIF2a control the cell identity also *in vivo* [59].

Beyond the impact of the mechanics on cell fate, we herein unveil the calcium homeostasis and the UPR signaling as a mechanical responsive pathway. Our results demonstrate that physiological mechanics is sufficient to rebalance the intracellular calcium concentration and triggers an ERS. These data are consistent with the central role played by the calcium flux to maintain a quiescent state. Interestingly, *in vivo*, modulation of the calcium efflux between the ER and the cytosol is sufficient for inducing cell proliferation [60,61]. During the recent years, the ER has emerged as an integration hub of mechanical cues. Indeed, IRE1 and PERK, two key ER sensors, physically interact with the filamin A and F-actin [62,63]. These interactions remodel the cytoskeleton and dictate the cell migration properties. However how the physical cues are integrated by the ER remains poorly described. Mechanical cues are sensed at focal adhesions, an integrin-based structure at the cell membrane. The ER-plasma membrane contact sites represent specific regions of interest for integration of the physical cues, organelle contacts and calcium signaling. Interaction of STIM1, anchored in the ER membrane, and ORAI1, located within the plasma membrane, promote calcium entry and limits the ER stress activity [64]. Assembly of the STIM1-ORAI1 complex is controlled by integrin signaling, notably the Wnt5a pathway, that might be influenced by the mechanical microenvironment [65]. Further investigations are required to elucidate the molecular crosstalk between the physical microenvironment, regulation of calcium homeostasis and the cell identity regulation. Our study also demonstrates that the mechanical environment protects against metabolic stress. Various pathologies combine profound rearrangements of the physical and

nutritional microenvironment. Indeed, tissue stiffening is often associated with defects in angiogenesis and alteration of the tissue perfusion. How diseased cells survive to scarcity constitutes key challenges in the understanding of the mechanisms underlying pathologies development. Consistent with our observation, multiple pathologies associate to physical changes of the tissue, also display an alteration of Ca^{2+} homeostasis and signaling associated to a decreased Ca^{2+} concentration within the ER lumen [66]. Additionally, antiapoptotic proteins such as BCL-2 reduces the concentration of Ca^{2+} in the ER providing resistance to apoptosis [67]. Consistently our results demonstrate that physiological stiffness and associated Ca^{2+} depletion is protecting against cell death caused lack of glucose and canonically attributed to a terminal ERS. This discrepancy of cell outcome upon stress depending on the stiffness of the extracellular environment cannot be attributed to a bias in glucose metabolism or nutrient exhaustion in the medium according to the substrate since cells were subjected to complete starvation at the same time. Thus, the protective effect observed on the soft substrate should be rather caused by mechanical-driven balancing of the Ca^{2+} concentration, priming progenitor cells to resist to a second ER stressors, limiting cell death of damaged cells and promoting disease development. So far, a large knowledge of regarding stress response comes from mechanistical investigations performed on 2D culture grown TCP, a rigid matter associated to aberrant proliferative rate and loss of cell identity. Revisiting these mechanisms on mechanomimetic supports, better reflecting the progenitor biology, would be a promising approach for the comprehension of cell outcome upon stresses and pathologies initiation and progression.

More generally, hits identification at early step of drug discovery or toxicology assessments and the wide acceptance of alternative models imply standardized and reliable cell culture methods compatible with prolonged exposure and high throughput screening. These requirements are, presently, not compatible with 3D models since spheroids/organoids are costly to produce at large scale, often heterogenous in shape and size with a poor number of stem cells that exhausts along few passages and difficult to monitor by conventional imaging systems [68]. Thus, the traditional 2D culture still remains the gold standard with well-known limitations, notably in terms of cell drift. Although commercial culture media have been developed which balance metabolic fluxes as closely as possible to the physiopathology [69,70], the bias caused by the extraphysiological rigidity of plastic or glass remains poorly considered. Our study however shows the determinant impact of the mechanics on calcium metabolism, cell identity and cell outcome upon stressors. They thus argue in favor of the implementation of the mechanical microenvironment for improving the identification of compounds of interest and higher prediction of toxicity.

Materials and methods

Fabrication of mechanomimetics multiwells plates

Six wells plates with hydrogel bottoms were designed by Cell&Soft company (Grenoble, France). In brief, polyacrylamide hydrogels were photo-polymerized onto glass slides of dimensions 78 x 112 mm^2 (Gataca Systems, Massy, France), following the protocol described in [71]. The duration of the UV exposure was chosen to achieve a stiffness close to 3 kPa. The gel was rinsed 3 times in deionized water to remove the unreacted compounds and left for swelling overnight. The gel was then dehydrated at room temperature. The plastic frame of a 6 wells bottom-less plate (Greiner Bio-One, Courtaboeuf, France, ref. 657160, home processed) was glued to the gel with a UV sensitive glue (NOA68, Norland Adhesives, Jamesburg, NJ, USA). NOA68 is based on polyurethane, a compound that is widely used in the medical industry. The surface of the gel was then rendered permissive to cell adhesion by coating Rat Tail collagen I (Gibco, Thermo Fisher Scientific, Whaltam, Massachusetts, USA, Ref. A10483-01) at a density of 1 µg/cm^2 using the heterobifunctional crosslinker sulfo-LC-SDA (sulfosuccinimidyl 6-(4,40 -azipentanamido)hexanoate,Pierce, Thermo Fisher Scientific, Courtaboeuf, France) at a concentration of 0.6 mg/ml. The solution was removed after 1h and the gel was dehydrated for 45 min at room temperature. The gel was then exposed to UV light (UV KUB1, 16 mW/cm^2, Kloe, Montpellier, France) for 5 min to bind the diazirine group to the polyacrylamide gel. A solution of collagen 1 at 12 µg/ml was deposited on the surface and evaporated at room temperature under agitation, allowing the reaction of the NHS group of the sulfo-LC-SDA with the protein. This led to the theoretical crosslinking of 1 µg/ cm^2 of Collagen I to the surface of the polyacrylamide hydrogel. The soft plate could be stored at 4°C up to three months. Culture treated plastic plates were coated with the same density of collagen I. Before use, the soft plate was extensively rinsed with PBS (Gibco, Thermo Fisher Scientific, Whaltam, Massachusetts, USA) and the gel was let for swelling 24 h at 4°C. PBS was replaced by culture medium 1 h before cell seeding, and the plates were placed at 37 °C in 5% CO_2.The stiffness of the hydrogel was characterized before assembly with the bottom-less frame using indentation-type AFM as described in [71].

Cell culture, starvation experiments and reagents

The HBEC-3KT cell line was obtained from ATCC. This cell line was cultured in Keratinocyte Serum Free media (KSFM; Ref 17005-034, GIBCO, Thermo Fisher Scientific, Whaltam, Massachusetts, USA) supplemented with Bovine Pituitary Extract 50mg.L^{-1} (Ref 13028-014, GIBCO, Thermo Fisher Scientific, Whaltam, Massachusetts, USA), glucose 16mM (Ref A24940-01, GIBCO, Thermo Fisher Scientific, Whaltam, Massachusetts, USA), recombinant human Epithelial Growth Factor 5µg.L^{-1} (Ref AF-100-15; PEPROTECH,

Thermo Fisher Scientific, Whaltam, Massachusetts, USA) and Penicillin/streptomycin Strep 1% (Ref 15140-122; GIBCO, Thermo Fisher Scientific, Whaltam, Massachusetts, USA).

Glucose starvation experiments were performed with Dulbecco's Modified Eagle Medium devoid of glucose and sodium pyruvate (Ref A1443001, GIBCO, Thermo Fisher Scientific, Whaltam, Massachussets, USA) and supplemented with penicillin/streptomycin 1% and 10% dialyzed FBS. The concentrations of nutrients were determined as previously described [72] : glucose 25 or 0mM (ref A2494001, GIBCO, Thermo Fisher Scientific, Whaltam, Massachussets, USA) and with the subsequent amino acids purchased from Sigma Aldrich (Saint Louis, Missouri, USA) : L-proline 0.15 mM (ref P5607), L-alanine 0.15 mM (ref 05129), L-aspartic acid 0.15 mM (ref A8949), L-glutamic acid 0.03 mM (ref W328502), L-asparagine 0.34 mM (ref A4159) and L-glutamine 2 mM (ref G3126).

ISRIB (ref SML0843, Sigma Aldrich, Saint Louis, Missouri, USA) was bought in powder and dissolved in DMSO to be later used at a final concentration of 400 nM. Thapsigargin (Ref TQ0302, TARGETMOL, Wellesley Hills, Massachusetts, USA) was dissolved in DMSO and then used at 1 µM.

Air-Liquide Interface differentiation assay

Air-Liquide Interface culture were performed according the recommendations from Stemcell technologies. In brief, cells were seeded at a density of $1.1x10^5$ cells/well onto a 12mm Transwell (ref 38023, STEMCELL TECHNOLOGIES, Saint Égrève, France) and grown in KSFM until cell confluency. Then cells were subjected to air-lift. KSFM was removed from the upper and lower chambers and differentiation medium was added to the lower chamber only to allow contact with air. Differentiation medium was prepared as recommended by the company: PneumaCult-ALI Basal Medium was mixed with Pneumacult-ALI supplement (10X), Pneumacult-ALI Maintenance Supplement (100X), Heparin 4 µg/mL (Ref 07980, Stemcell technologies, Saint Égrève, France) and Hydrocortisone 480 ng/mL (Ref 07925, Stemcell technologies, Saint Égrève, France). Differentiation was monitored daily and differentiation medium was carefully changed every 2 days for 21 days. Differentiated ALI Culture of HBEC-3KT cells were then formalin-fixed, embedded in paraffin and processed for hematoxylin and eosin staining at the CRCL anatomopathological facility.

Cell cycle analysis

HBEC-3KT cells were plated (1×10^5 cells/well) on TCP or 3kPa plates and grown for 3 days. Then cells were treated with ISRIB (400 nM) or vehicle for 3 days. Cells were trypsinized, washed with PBS and centrifuged at 300 g for 5 mins. They were then counted and fixed in cold 70% ethanol for at least 2 hours on ice and pelleted. Cells were resuspended at 1×10^6 cells/ml in staining solution, Hank's buffered saline solution

containing 4 ug/ml of Hoechst 33342 (Ref B2261, Sigma Aldrich, Saint Louis, Missouri, USA) for 1 h in the dark at 4°C cells. Stained cells were analyzed using a BD LSRFortessa™ flow Cytometer (BD Biosciences, Le Pont de Claix, France), and cell cycle distributions were determined with FlowJo software (Ashland, OR, USA).

Senescence-associated beta-galactosidase test

HBEC-3KT cells were plated (1 x 10^5 cells/well) on TCP or 3 kPa plates and grown for 3 days. Cells were fixed in 0.5% glutaraldehyde solution (ref 49629, Sigma Aldrich, Saint Louis, Missouri, USA) for 10 minutes. beta-galactosidase solution was prepared containing 20 mM citric acid (pH=6)(ref 1.00244.0500, Merck Millipore, Darmstadt, Germany), 5 mM of potassium hexacyano-ferrate (II) trihydrate (ref 1.04894, Merck Millipore, Darmstadt, Germany), 5 mM of potassium hexacyano-ferrate (III) (ref1 .04973, Merck Millipore, Darmstadt, Germany), 2 mM of magnesium chloride (ref 1.05833, Merck) 150 mM of Sodium Chloride (ref S3014, Sigma Aldrich, Saint Louis, Missouri, USA) and 1 mg/ml X-Gal (ref EU0012-D, Euromedex, Souffelweyersheim, France) previously resuspended in N-N' dimethylformamide. After fixation, cells were washed with beta gal solution to adjust cellular pH. Cells were incubated with beta gal solution and covered with aluminum for 6 hours at 37°C. Cells were then washed with PBS and nuclei was stained with Hoechst 33342 (Ref B2261, Sigma Aldrich, Saint Louis, Missouri, USA). Positive beta-gal cells were then quantified and percentage was assessed using total nuclei number.

Intracellular calcium detection

HBEC-3KT cells were plated (1 x 10^5 cells/well) on TCP or 3kPa plates and grown for 3 days. Fluo-4AM Solution (Ref FP-132303, Interchim, Montlucon, France) was prepared diluting Fluo-4AM (final concentration of 2µM) in 1:1 PBS-KSFM medium. Cells were then incubated with the mixture for 30 minutes and washed with Hank's buffered saline solution (HBSS) for 30 minutes prior to imaging. The DPX blue/white ER-Tracker (ref 12353, Thermo Fisher Scientific, Whaltam, Massachussets, USA) was used to visualize the endoplamic reticulum in live cells. Images were acquired using Axio Vert.A1 microscope (ZEISS, Munich, Germany).

Cell Proliferation, cellular motility and cytotoxicity assay

For cell proliferation, HBEC-3KT cells were plated onto 6-well plate (1 x 10^5 cells per well). Cell confluency was monitored and quantified over time using the Cellcyte X system (Cytena, Freiburg im Breisgau,

Germany). Cells were also followed every 15 minutes over 2-hour long period to quantify cellular motility using the TrackMate Plugin for Fiji/ImageJ software (National Institutes of Health, Bethesda, Maryland, USA).

For cell death assessment, HBEC-3KT (1x10^{5}cells/well) were seeded onto TCP or 3kPa 6-well plate and grown for 3 days. Then cells were subjected to indicated deprivation. Propidium iodide was added in the media at 2.5 µg/ml. Then, cell confluency and cell death were monitored over the indicated period of time using the Cellcyte X system (Cytena, Freiburg im Breisgau, Germany). Death index was calculated using the formula "(PI Foci Number/Confluency) x100".

RNA extraction and RT-qPCR

Total cellular RNA was extracted after the indicated period of treatment using TRIzol Reagent (ref 15596026, Invitrogen, Carlsbad, California, USA) according to the manufacturer's protocol. For cDNA synthesis, 0.25 µg of RNA were reverse transcribed using Superscript II reverse transcriptase (ref 18064014, Invitrogen, Carlsbad, California, USA) with random primers (S0142, Thermo Fisher Scientific, Whaltam, Massachussets, USA), according to the manufacturer's instructions. cDNA was then amplified by qPCR using specific primers listed in supplementary Table 1 and the SYBR Green Master Mix (ref 1725274, Bio-Rad, Hercules, California, USA). qPCR was performed using the CFX connect real-time PCR system (Bio-Rad, Hercules, California, USA). Relative quantification was determined by using the delta-CT method. Expression of target genes was normalized against RPS11 mRNA levels used as an internal control. QPCR experiments were repeated at least three times in duplicate.

Western blot analysis and SUnSET assays

To perform Western blot analysis, cells were platted on TCP or 3kPa plates (1 x 10^5 cells/well) and grown for 3 days. Whole cell extracts were prepared from cultured cells lysed at 4°C in RIPA protein buffer containing protease and phosphatase inhibitors (ref 11697498001, Roche, Basel, Switzerland), and obtained by centrifugation at 13,000 g for 20 min at 4°C.

Protein concentrations of the cellular extracts were determined using the DC Protein Assay (ref 5000112, Bio-Rad, Hercules, California, USA). Equal amounts of proteins (20 µg) were separated by SDS-PAGE and then transferred onto nitrocellulose membranes (ref 1704271, Bio-Rad, Hercules, California, USA). Membranes were incubated in blocking buffer, 5% milk or Bovine Serum Albumin (BSA) in Tris-Buffered Saline/Tween 20 (TBST), for 1 h at room temperature, then incubated overnight at 4°C with the appropriate primary antibodies diluted in TBST containing 5% milk or BSA. Membranes were washed three times with

TBST, incubated for 1 h at room temperature with the appropriate secondary antibodies, diluted in TBST containing 5% milk, and again washed three times with TBST. Detection by enhanced chemiluminescence was performed using the Immobilon Forte HRP Western substrate (ref WBLUF0500, Merck Millipore, Darmstadt, Germany) or SuperSignal West Femto Maximum Sensitivity Substrate (ref 34096, Thermo Scientific, Thermo Fisher Scientific, Whaltam, Massachussets, USA). Red Ponceau was used as a loading control. The primary antibodies used were purchased from Bethyl laboratories: P-KAP1 (A300-2575A), from Cell Signaling Technology (Danvers, Massachussets, USA): P-CHK1 (2348), Gamma H2AX (2577), CD98 (13180), BiP (3177), P-eIF2a (3398), ATF4 (11815), P-S6 (4858), from Merck Millipore (Darmstadt, Germany): P-ATM (05-740), Puromycin clone 12D10 (MABE343). The HRP-conjugated secondary antibodies (anti-rabbit and anti-mouse antibodies, respectively ref 7074 and 7076) were supplied by Cell Signaling Technologies (Danvers, Massachussets, USA).

Nascent protein synthesis were evaluated using the surface sensing of translation (SUnSET) method as previously described by Schmidt et al. [73]. 15 min before being harvested and processed to prepare whole cell extracts in RIPA buffer, cells were incubated with 5 µg/mL of puromycin (ref P9620, Sigma Aldrich, Saint Louis, Missouri, USA) directly added into the medium. The amount of puromycin incorporated into nascent peptides was then evaluated by Western blot analysis on 20 µg of proteins using anti-puromycin antibody (ref MABE343) purchased from Merck Millipore (Darmstadt, Germany).

Immunofluorescence staining

The surface density of the collagen I was controlled by immunofluorescence using an Alexa Fluor 488 conjugated polyclonal antibody against the collagen I A1 (bs-10423R-A488, Cliniscience, Nanterre, France). Depth stacks obtained with confocal microscopy (Zeiss LSM880) were used as described in [74].

For aggresome assessment, HBEC-3KT cells were plated (1 x 10^5 cells/well) on TCP or 3kPa plates and grown for 3 days. Then cells were fixed in fixed in 4% of paraformaldehyde in phosphate-buffered saline (PBS) before permeabilization with 0.5% Triton X-100 in PBS and stained with primary antibodies: anti-Ki67 (M7240, Agilent Dako, Santa Clara, CA, USA) diluted at 1/50 and anti-Poly-ubiquitin purchased from ENZO (ENZ-ABS840, Villeurbanne, France) diluted at 1/650. Secondary Antibody Alexa Fluor 488 Goat anti-mouse IgG (ref A-11029, Life Technologies, Carlsbad, California, USA) was used at 1:600. Nucleus were stained for 5 min with Hoechst n°33342 (ref H3570, Invitrogen, Carlsbad, California, USA) at 1:2000. Plates were mounted using the Fluoromount G mounting medium (ref 17984-25, EMS Diasum, Hatfield, Pennsylvania, USA). For Ki-67 staining, fluorescence microscope (Axio Vert.A1, ZEISS, Munich, Germany) was used to acquire image. For

poly-Ubiquitin staining, ZEISS Confocal imager (40X) Zeiss LSM 880 was uses. Final images were analyzed and cropped with the Fiji/ImageJ software (National Institutes of Health, Bethesda, Maryland, USA).

RNA sequencing

For RNA sequencing, HBEC-3KT Cells were cultured for 2 (P2) or 20 (P20) passages onto TCP or 3kPa plates and grown for 3 days. RNA was extracted using NucleoSpin RNA kit (Macherey-Nagel, Düren, Germany). Library preparation and RNA sequencing were performed at the ProfileXpert platform (Université Claude Bernard of Lyon, Lyon). Quality of samples was checked by Bioanalyzer 2100 (Agilent) and RNA was quantified by Quantifluor RNA kit (Promega, Charbonnières-les-bains, France). First, mRNA was enriched from 1 µg of total RNA, then library preparation was realized with the NextFlex Rapid Directional mRNA-Seq kit (Bio-Scientific, Perkin-Elmer, Villebon-sur-Yvett, France). Quality of libraries were checked by Fragment Analyzer (Agilent) and quantified by qPCR. Samples were put on Flow Cell High Output. Amplification and sequencing were performed with Illumina NextSeq500: run Single Read 76 bp was performed. After demultiplexing of the data with Bcl2fastq v2.17.1.14 (Illumina Inc, San Diego, CA, USA). Reads where mapped using Bowtie 2 on the human genome GRCh38 and counted using htseq count in the Galaxy project platform [75]. Differentially expressed genes were identified using DESeq2 and volcano plot were generated in ExpressAnalyst platform. All enrichment analysis were performed in ExpressAnalyst platform [76].

Single-cell data analysis

Already annotated, normal human single-cell RNA sequencing data set ("facs_normal_lung_blood_scanpy.20200205.RC4.h5ad") were downloaded from https://www.synapse.org/#!Synapse:syn21560554 [49]. The scanpy object contained 9409 cells obtained during surgery from three patients undergoing lobectomy, including epithelial, endothelial, immune, and stromal cells. The sampled tissue corresponded to histologically normal lung tissue (bronchi, bronchiole, and alveolar regions), along with peripheral blood. Data were processed using R 4.2.0 and RStudio 2022.12.0+353. Downloaded scanpy object (.h5ad) was converted into a Seurat v4 object (.RDS) using "anndata" 0.7.5.6 and "Seurat" 4.3.0, prior to subsetting the cells of interest ("subset" function of Seurat)[77–79]. Cells of interest were represented by basal cells (three clusters, one from each patient), differentiating basal cells (one cluster), and ciliated cells (three clusters, one from each patient). We processed the new object using "Seurat" package, as follows: normalization ("NormalizeData" function), identification of highly variable features ("FindVariableFeatures" function), scaling the data ("ScaleData" function, performed on all the genes), linear dimensional reduction ("RunPCA" function), and non-linear dimensional reduction ("RunTSNE" function). All

the clusters corresponding to the same cell type (for example, the three clusters of basal cells) were merged using the "RenameIdents" function. The t-distributed stochastic neighbor embedding (t-SNE) reduction was visualized using the "DimPlot" function. Differentially expressed features were calculated for each of the three cell types with the "FindAllMarkers" function, using the following parameters: only.pos = TRUE, min.pct = 0.25, logfc.threshold = 0.25, and kept only genes with an adjusted p-value <0.05. Then, we used "EnrichR" and "Enrichr Appyter" to identify and visualize top enriched terms [80,81]. Unfolded protein response gene signature was analyzed and plotted with "Single-Cell Signature Explorer" (https://sites.google.com/site/fredsoftwares/products/single-cell-signature-explorer). First, with the "Single-Cell Signature Scorer" software, we computed for each cell a signature score based on the "HALLMARK_UNFOLDED_PROTEIN_RESPONSE" signature from the "The Molecular Signatures Database". Then, we used the "Single-Cell Signature Merger" software to collate the signature scores table with t-SNE coordinates, and, finally, the "Single-Cell Signature Viewer" software to display on a t-SNE map the signature scores .

Statistics

All of the statistical analyses were performed using GraphPad Prism version 6.0 (GraphPad Software, San Diego, CA, USA) by using Student's t-test, Paired t-test, One-Way ANOVA or Two-way ANOVA and post-hoc Tukey multi-comparisons test. p-values less than 0.05 were considered statistically significant. Absence of mark "*" indicates lack of statistical significance.

Acknowledgements

We thank the D Bernard's lab for technical assistance in senescence assessment and sharing reagents, B. Manship for English editing and Y. Chaix for funding management. The authors are grateful to the members of the Imagerie Cellulaire, cytometry and ProfileXpert facilities for their collaborative work. This work was supported by the ANR (ANR-22-CE51-0043-01) and INCa (PLBIO22-227), Cancéropôle CLARA (CVPPRCAN000174, CVPPRCAB000180 and CV-2021-039), Region Auvergne Rhone-Alpes (19-010898-01), Ligue Nationale contre le Cancer (R23031CC, R19007CC), Institut Convergence François Rabelais (17IA66ANR-PLASCAN-MEHLEN). A.N. acknowledges the support of the French Renatech network. A.N, C.M. and C.H. thank the microscopy facility MuLife of IRIG/DBSCI, funded by CEA Nanobio and GRAL LabEX (ANR-10-LABX-49-01) financed within the University Grenoble Alpes graduate school CBH-EUR-GS (ANR-17-EURE-0003).

Declaration of interests: A. N, C. M. are shareholders of the Cell&Soft company.

Supplementary information: Supplementary figures 1, 2 and 3, Supplementary table 1

Author contributions

PA L: Data curation, Methodology, Software., M P: Data curation, Methodology., P LG: Data curation, Methodology., M I: Data curation, Methodology, Validation., J F: Data curation, Methodology, Validation., I C: Supervision, Investigation., T R: Supervision, Investigation., N A: Validation Supervision, Investigation., S A: Validation, Supervision, Investigation., C H: Data curation, methodology. C M: Data curation, methodology, C D: Data curation, Methodology, Validation, Investigation., P B: Data curation, Methodology, Investigation., C FP: Validation Supervision, Investigation., A N: Data curation, methodology, conceptualization, funding acquisition, Writing-Original draft preparation., C C: Conceptualization, supervision, funding acquisition, Writing- Original draft preparation.

Figure legends

Fig. 1. Design of multiwell plates with homogenous pulmonary stiffness across wells.

A. A 40 µm thick layer of polyacrylamide prepolymer solution is UV-cured on a large glass slide.
B. The hydrogel coated glass is further bonded to a bottom-less plate with a liquid adhesive that penetrates in the depth of the hydrogel and makes a physical barrier between the wells.
C. Stiffness characterization of the soft bottom in each well. Young's modulus: 3.3 +/- 0.5 kPa.
D. Relative variation of the surface density of the collagen 1 that is grafted onto the hydrogel in each well. Variation is of +/- 0.13.

Fig. 2. Soft hydrogels hinder human bronchoepithelial cells proliferation

A. Schematic representation of serial passages done on either Tissue Culture Plastic (TCP) or 3kPa hydrogel.
B. Pictures from HBEC-3KT cells grown on either TCP or 3kPa stiffnesses and followed over 4 days.
C. Cell proliferation measurement of HBEC-3KT cells grown on either TCP or 3kPa stiffnesses confluency over 4 days of culture. Data are expressed as mean +/- s.e.m of independent experiments (n = 3), Two-way ANOVA and Tukey's multiple comparisons test were performed (***p < 0.001).
D. Quantification of the proliferative subpopulation (Ki67-positive cells) of HBEC-3KT cells cultured on either TCP or 3kPa stiffnesses for 2 days. Data are expressed as mean +/- s.e.m of independent experiments (n = 3), Student's t-test, *** p < 0.001.
E. Cell velocity measurement of HBEC-3KT cells cultured on either TCP or 3kPa stiffnesses for 2 hours. Distribution is shown as violin plot. Data are expressed as mean +/- s.e.m of independent experiments (n = 3), Student's t-test.
F. Doubling time measurement of HBEC-3KT cells grown on either TCP or 3kPa stiffnesses over 20 passages. Data are expressed as mean +/- s.e.m of independent experiments (n = 3), Student's t-test, * p < 0.05.

Fig. 3. Pulmonary soft hydrogel induces a reversible quiescence stage in S-phase.

A. Cell area measurement of HBEC-3KT cells grown on TCP or 3kPa stiffnesses. After 2 days of culture on both supports, cell edges were delimitated (outline in red, right panel) and cellular area were measured (left panel). Data are expressed as mean +/- s.e.m of independent experiments (n = 3). Student's t-test (*p < 0.05)
B. Gene expression analysis of canonical markers of quiescence and senescence *P16*, *P21, P27, EZH1* and *FOXO3A* in cells grown on either TCP or 3kPa stiffnesses. Data are expressed as mean +/- s.e.m of independent experiments (n = 4), unpaired two-tailed t test (*p<0.05; **p< 0.01; ***p<0.001).
C. Senescence measurement of HBEC-3KT cells cultured on TCP or 3kPa stiffnesses. After 2 days of culture, SA-β-galactosidase assay was performed, and cells were imaged (left panel). The percentages of positive cells were quantified (right panel). Data are expressed as mean +/- s.e.m of independent experiments (n = 3), Student's t-test, (*p<0.05)
D. Cell cycle analysis by flow cytometry of cells cultured on TCP or 3kPa stiffnesses. Cell distribution was plotted according to DNA content (left panel) and quantification of each cell cycle groups was assessed (right panel). Data are expressed as mean +/- s.e.m of independent experiments (n = 3), paired two-tailed t test (**p< 0.01)
E. Quiescence reversibility assay of HBEC-3KT cells according to the described conditions. Cells were seeded on either TCP or 3kPa stiffnesses and then cross-platted following the schematic (left panel). Confluency was then assessed over 48 hours using live-imaging system. Data are expressed as mean +/- s.e.m of independent experiments (n = 3). Two-way ANOVA and Tukey's multiple comparisons test were performed. Only the final time point statistics is presented (*p<0.05; **p< 0.01)0

Fig. 4. Pulmonary soft hydrogel retains cell differentiation capabilities over high number of passages

A. Schematic representation of Air-Liquide Interface (ALI) culture of HBEC-3KT Cells cultured over short (2 passages) or long (20 passages) periods of time on Tissue Culture Plastic (TCP) or 3kPa plates.

B. HBEC-3KT cells were imaged before air-lift (induction of differentiation) for each condition (left panel) and cell area was measured (right panel). Data are expressed as mean +/- s.e.m of independent experiments (n = 3), student t test (***p<0.001)
C. RT-qPCR analysis of progenitor markers *KRT5*, *KRT14* and *TP63* in HBEC-3KT cells pre-cultured on either TCP or 3kPa plates and seeded in ALI membranes (before airlift). Data are expressed as mean +/- s.e.m of independent experiments (n = 3), one-way ANOVA and Tukey's multiple comparisons test (**p< 0.01; ***p<0.001).
D. ALI cultures of HBEC-3KT cells were imaged after 21 days of differentiation and stained with Hematoxylin-Eosin (HE), highlighting alveolar-like structures. Quantification of the alveoli area are indicated on the right panel. Data are expressed as mean +/- s.e.m of independent experiments (n = 3), student t test (***p<0.001).
E. RT-qPCR analysis of alveolar cell markers *PDPN* and *ACE2* in HBEC-3KT ALI culture 14 days post air-lift. Relative fold increase was assessed based on passage number. Data are expressed as mean +/- s.e.m of independent experiments (n = 3), student t test (*p< 0.05; ***p<0.001).

Fig. 5. Pulmonary soft hydrogel does not trigger DNA damages but impairs translational processes and protein synthesis

A. Western blot analysis of markers of the DNA-damage repair (DDR) signaling pathways in HBEC-3KT cells cultured on TCP or 3kPa. Phosphorylated forms of ATM (p-ATM), KAP1 (p-KAP1) and H2AX (γ-H2AX) were used as markers the ATM pathway. Phosphorylated Ser345 of Chk1 (p-Chk1) was used as a reflect of the ATR axis. Cells grown on TCP and treated with etoposide (TCP Eto, 3 hours) were used as a positive control. Ponceau red staining was used as loading control.
B. Schematic representation of the transcriptome analysis performed in HBEC-3KT cells cultured on either TCP or 3kPa supports.
C. Volcano Plot of the differentially expressed genes (3kPa vs TCP, HBEC-3KT passage P2). Significantly downregulated genes are highlighted in blue while upregulated genes are in red.
D. Ridgeline plots of the 10 most significantly enriched pathways.
E. Heatmap Plot based on Translational Initiation gene signature for each condition.
F. GSEA enrichment plot of the translation initiation gene signature.
G. Protein synthesis measurement by SUnSET assay of HBEC-3KT cells cultured on TCP or 3kPa supports. Ponceau red Staining was used as loading control.

Fig. 6. Pulmonary soft hydrogel rebalances Ca^{2+} concentration in the endoplasmic reticulum and triggers a basal ER stress.

A. Western blot analysis of canonical ER stress markers (phospho-eIF2a, ATF4 and BiP) in HBEC-3KT cells cultured on TCP or 3kPa plates for 3 days. Ponceau red staining was used as loading control.
B. Gene expression analysis of ER stress target genes *ASNS, TRIB3, CHOP* and *P58^{IPK}* in cells seeded on TCP or 3kPa support. Data are expressed as mean +/- s.e.m of independent experiments (n = 4), Student's t-test (*p< 0.05; **p<0.01).
C. Analysis of aggresome formation in HBEC-3KT cells cultured on TCP or 3kPa supports. Immunofluorescence staining against poly-ubiquitin was performed after 3 days of cell culture. Hoechst dye was used to stain nuclei.
D. Western blot analysis of CD98 N-glycosylation in cells cultured on TCP or 3kPa plates for 3 days. HBEC-3KT grown on TCP and then deprived for glucose (24 hours) were used as a positive control. Ponceau red staining was used as a loading control.
E. Gene expression analysis of ER stress markers (*ASNS, TRIB3, CHOP, P58^{IPK}*) in HBEC-3KT cells grown on TCP or 3kPa for 3 days with daily medium refreshment. Data are expressed as mean +/- s.e.m of independent experiments (n = 4), Student's t-test (*p< 0.05; **p<0.01).
F. Assessment of the intracellular calcium concentration in HBEC-3KT cells grown on TCP or 3kPa. After 3 days of culture, Ca^{2+} was stained using the Fluo-4AM dye (right panel). Relative fluorescence intensity was quantified (right panel). Data are expressed as mean +/- s.e.m of independent experiments (n = 3), student's t-test (***p< 0.001).

Fig. 7. ISRIB treatment favors the S/G2 transition and soft matrix confers resistance to glucose deprivation.

A. Gene expression analysis of *TRIB3, ASNS, CHOP, P58^{IPK}, P16, P21, P27, FOXO3A* in HBEC-3KT cells platted in TCP or 3kPa and treated with or without ISRIB (400nM, 3 days). Data are expressed as mean +/- s.e.m of independent experiments (n = 8), One-way ANOVA and Tukey's multiple comparisons test (*p< 0.05; **p<0.01, ***p<0.001).
B. Cell cycle analysis by flow cytometry of cells cultured on 3kPa stiffness with or without ISRIB (400nM, 3 days). Cell distribution was plotted according to DNA content (left) and quantification of each cell cycle groups was assessed (right). Data are expressed as mean +/- s.e.m of independent experiments (n = 3), paired two-tailed t-test (**p< 0.01)
C. Measurement of glucose starvation-induced cell death in HBEC-3KT cells grown on TCP or 4kPa stiffnesses. Following 3 days of culture, cells were subjected to media with or without glucose (25 vs 0mM) for 48 hours. At end point, dead cells were stained using propidium iodide and imaged (Bf=brightfield, PI=propidium iodide). Death index was quantified in each condition (bottom). Data are expressed as mean +/- s.e.m of independent experiments (n = 3), One-way ANOVA and Tukey's multiple comparisons test (*p< 0.05).
D. Gene expression analysis of ATF4-dependent proapoptotic genes (c*FOS, TRIB3, CHOP*) in HBEC-3KT cells grown on TCP or 3kPa and starved for glucose for 48 hours. Data are expressed as mean of fold change +/- s.e.m of independent experiments (n = 3), Student's t-test (*p< 0.05; **p<0.01).

Fig. 8. Pulmonary basal cells in human tissue exhibit marks of dysregulated translation and an active unfolded protein response.

A. Bar chart of the top 10 enriched terms from the "GO_Biological_Process_2021" gene set library for basal, differentiating basal and ciliated cells. The enriched terms are displayed based on the -log10(p-value). The actual p-value is indicated next to each enriched term.
B. t-SNE map depicting normal human basal cells (in red, 240 cells), differentiating basal cells (in blue, 43 cells), and ciliated cells (in green, 551 cells) (top panel). Visualization of the "unfolded protein response" signature (113 genes) in the t-SNE map of the 843 human cells represented above (bottom panel).

References

1. Carley, E., King, M.C., and Guo, S. (2022). Integrating mechanical signals into cellular identity. Trends Cell Biol *32*, 669–680. 10.1016/j.tcb.2022.02.006.
2. Shiraishi, K., Shah, P.P., Morley, M.P., Loebel, C., Santini, G.T., Katzen, J., Basil, M.C., Lin, S.M., Planer, J.D., Cantu, E., et al. (2023). Biophysical forces mediated by respiration maintain lung alveolar epithelial cell fate. Cell *186*, 1478-1492.e15. 10.1016/j.cell.2023.02.010.
3. Kureel, S.K., Mogha, P., Khadpekar, A., Kumar, V., Joshi, R., Das, S., Bellare, J., and Majumder, A. (2019). Soft substrate maintains proliferative and adipogenic differentiation potential of human mesenchymal stem cells on long-term expansion by delaying senescence. Biol Open *8*, bio039453. 10.1242/bio.039453.
4. Heo, S.-J., Szczesny, S.E., Kim, D.H., Saleh, K.S., and Mauck, R.L. (2018). Expansion of mesenchymal stem cells on electrospun scaffolds maintains stemness, mechano-responsivity, and differentiation potential. J Orthop Res *36*, 808–815. 10.1002/jor.23772.
5. Ben-David, U., Siranosian, B., Ha, G., Tang, H., Oren, Y., Hinohara, K., Strathdee, C.A., Dempster, J., Lyons, N.J., Burns, R., et al. (2018). Genetic and transcriptional evolution alters cancer cell line drug response. Nature *560*, 325–330. 10.1038/s41586-018-0409-3.
6. Belaadi, N., Pernet, L., Aureille, J., Chadeuf, G., Rio, M., Vaillant, N., Vitiello, E., Lafanechère, L., Loirand, G., and Guilluy, C. (2022). SUN2 regulates mitotic duration in response to extracellular matrix rigidity. Proc. Natl. Acad. Sci. U.S.A. *119*, e2116167119. 10.1073/pnas.2116167119.
7. Mih, J.D., Sharif, A.S., Liu, F., Marinkovic, A., Symer, M.M., and Tschumperlin, D.J. (2011). A Multiwell Platform for Studying Stiffness-Dependent Cell Biology. PLoS ONE *6*, e19929. 10.1371/journal.pone.0019929.
8. Tschumperlin, D., Liu, F., and Mih, J. Compliant surface multi-well culture plate.
9. Ahmed, N., Schober, J., Hill, L., and Zustiak, S.P. (2016). Custom Multiwell Plate Design for Rapid Assembly of Photopatterned Hydrogels. Tissue Engineering Part C: Methods *22*, 543–551. 10.1089/ten.tec.2015.0522.
10. Janmey, P.A., Fletcher, D.A., and Reinhart-King, C.A. (2020). Stiffness Sensing by Cells. Physiological Reviews *100*, 695–724. 10.1152/physrev.00013.2019.
11. Sun, X., Zhang, H., He, J., Cheng, R., Cao, Y., Che, K., Cheng, L., Zhang, L., Pan, G., Ni, P., et al. (2018). Adjustable hardness of hydrogel for promoting vascularization and maintaining stemness of stem cells in skin flap regeneration. Applied Materials Today *13*, 54–63. 10.1016/j.apmt.2018.08.007.
12. Rustad, K.C., Wong, V.W., Sorkin, M., Glotzbach, J.P., Major, M.R., Rajadas, J., Longaker, M.T., and Gurtner, G.C. (2012). Enhancement of mesenchymal stem cell angiogenic capacity and stemness by a biomimetic hydrogel scaffold. Biomaterials *33*, 80–90. 10.1016/j.biomaterials.2011.09.041.
13. Rumman, M., Dhawan, J., and Kassem, M. (2015). Concise Review: Quiescence in Adult Stem Cells: Biological Significance and Relevance to Tissue Regeneration. Stem Cells *33*, 2903–2912. 10.1002/stem.2056.
14. Marescal, O., and Cheeseman, I.M. (2020). Cellular Mechanisms and Regulation of Quiescence. Dev Cell *55*, 259–271. 10.1016/j.devcel.2020.09.029.
15. Laporte, D., Lebaudy, A., Sahin, A., Pinson, B., Ceschin, J., Daignan-Fornier, B., and Sagot, I. (2011). Metabolic status rather than cell cycle signals control quiescence entry and exit. J Cell Biol *192*, 949–957. 10.1083/jcb.201009028.
16. Otsuki, L., and Brand, A.H. (2018). Cell cycle heterogeneity directs the timing of neural stem cell activation from quiescence. Science *360*, 99–102. 10.1126/science.aan8795.
17. Wei, W., Nurse, P., and Broek, D. (1993). Yeast cells can enter a quiescent state through G1, S, G2, or M phase of the cell cycle. Cancer Res *53*, 1867–1870.
18. Vu, T.T.T., Lim, C., and Lim, M. (2012). Characterization of leukemic cell behaviors in a soft marrow mimetic alginate hydrogel. J Biomed Mater Res B Appl Biomater *100*, 1980–1988. 10.1002/jbm.b.32765.

19. Donker, L., Houtekamer, R., Vliem, M., Sipieter, F., Canever, H., Gómez-González, M., Bosch-Padrós, M., Pannekoek, W.-J., Trepat, X., Borghi, N., et al. (2022). A mechanical G2 checkpoint controls epithelial cell division through E-cadherin-mediated regulation of Wee1-Cdk1. Cell Rep *41*, 111475. 10.1016/j.celrep.2022.111475.
20. Almanza, A., Carlesso, A., Chintha, C., Creedican, S., Doultsinos, D., Leuzzi, B., Luís, A., McCarthy, N., Montibeller, L., More, S., et al. (2019). Endoplasmic reticulum stress signalling - from basic mechanisms to clinical applications. FEBS J *286*, 241–278. 10.1111/febs.14608.
21. Zhu, M., Zhou, S., Huang, Z., Wen, J., and Li, H. (2016). Ca2+-Dependent Endoplasmic Reticulum Stress Regulates Mechanical Stress-Mediated Cartilage Thinning. J Dent Res *95*, 889–896. 10.1177/0022034516640206.
22. Levental, I., Georges, P.C., and Janmey, P.A. (2007). Soft biological materials and their impact on cell function. Soft Matter *3*, 299–306. 10.1039/B610522J.
23. Sicard, D., Haak, A.J., Choi, K.M., Craig, A.R., Fredenburgh, L.E., and Tschumperlin, D.J. (2018). Aging and anatomical variations in lung tissue stiffness. American Journal of Physiology-Lung Cellular and Molecular Physiology *314*, L946–L955. 10.1152/ajplung.00415.2017.
24. Suki, B., Ito, S., Stamenovic, D., Lutchen, K.R., and Ingenito, E.P. (2005). Biomechanics of the lung parenchyma: critical roles of collagen and mechanical forces. J Appl Physiol (1985) *98*, 1892–1899. 10.1152/japplphysiol.01087.2004.
25. Cha, S.-I., Groshong, S.D., Frankel, S.K., Edelman, B.L., Cosgrove, G.P., Terry-Powers, J.L., Remigio, L.K., Curran-Everett, D., Brown, K.K., Cool, C.D., et al. (2010). Compartmentalized expression of c-FLIP in lung tissues of patients with idiopathic pulmonary fibrosis. Am J Respir Cell Mol Biol *42*, 140–148. 10.1165/rcmb.2008-0419OC.
26. Lanz, M.C., Zatulovskiy, E., Swaffer, M.P., Zhang, L., Ilerten, I., Zhang, S., You, D.S., Marinov, G., McAlpine, P., Elias, J.E., et al. (2022). Increasing cell size remodels the proteome and promotes senescence. Mol Cell *82*, 3255-3269.e8. 10.1016/j.molcel.2022.07.017.
27. McConnell, A.M., Yao, C., Yeckes, A.R., Wang, Y., Selvaggio, A.S., Tang, J., Kirsch, D.G., and Stripp, B.R. (2016). p53 Regulates Progenitor Cell Quiescence and Differentiation in the Airway. Cell Rep *17*, 2173–2182. 10.1016/j.celrep.2016.11.007.
28. Kippin, T.E., Martens, D.J., and van der Kooy, D. (2005). p21 loss compromises the relative quiescence of forebrain stem cell proliferation leading to exhaustion of their proliferation capacity. Genes Dev *19*, 756–767. 10.1101/gad.1272305.
29. Saldivar, J.C., Hamperl, S., Bocek, M.J., Chung, M., Bass, T.E., Cisneros-Soberanis, F., Samejima, K., Xie, L., Paulson, J.R., Earnshaw, W.C., et al. (2018). An intrinsic S/G2 checkpoint enforced by ATR. Science *361*, 806–810. 10.1126/science.aap9346.
30. ATM Regulates DNA Replication in Response to Stress (2014). Cancer Discovery *4*, OF9–OF9. 10.1158/2159-8290.CD-RW2013-261.
31. Sun, B., Ross, S.M., Rowley, S., Adeleye, Y., and Clewell, R.A. (2017). Contribution of ATM and ATR kinase pathways to p53-mediated response in etoposide and methyl methanesulfonate induced DNA damage. Environ Mol Mutagen *58*, 72–83. 10.1002/em.22070.
32. Neill, G., and Masson, G.R. (2023). A stay of execution: ATF4 regulation and potential outcomes for the integrated stress response. Front. Mol. Neurosci. *16*, 1112253. 10.3389/fnmol.2023.1112253.
33. Lee, D., Hokinson, D., Park, S., Elvira, R., Kusuma, F., Lee, J.-M., Yun, M., Lee, S.-G., and Han, J. (2019). ER Stress Induces Cell Cycle Arrest at the G2/M Phase Through eIF2α Phosphorylation and GADD45α. Int J Mol Sci *20*, 6309. 10.3390/ijms20246309.
34. Stockwell, S.R., Platt, G., Barrie, S.E., Zoumpoulidou, G., Te Poele, R.H., Aherne, G.W., Wilson, S.C., Sheldrake, P., McDonald, E., Venet, M., et al. (2012). Mechanism-based screen for G1/S checkpoint activators identifies a selective activator of EIF2AK3/PERK signalling. PLoS One *7*, e28568. 10.1371/journal.pone.0028568.
35. Lebeau, P.F., Platko, K., Byun, J.H., and Austin, R.C. (2021). Calcium as a reliable marker for the quantitative assessment of endoplasmic reticulum stress in live cells. J Biol Chem *296*, 100779. 10.1016/j.jbc.2021.100779.

36. Horn, M., Denzel, S.I., Srinivasan, B., Allmeroth, K., Schiffer, I., Karthikaisamy, V., Miethe, S., Breuer, P., Antebi, A., and Denzel, M.S. (2020). Hexosamine Pathway Activation Improves Protein Homeostasis through the Integrated Stress Response. iScience *23*, 100887. 10.1016/j.isci.2020.100887.
37. Console, L., Scalise, M., Salerno, S., Scanga, R., Giudice, D., De Bartolo, L., Tonazzi, A., and Indiveri, C. (2022). N-glycosylation is crucial for trafficking and stability of SLC3A2 (CD98). Sci Rep *12*, 14570. 10.1038/s41598-022-18779-4.
38. Simon, V.R., and Moran, M.F. (2001). SERCA activity is required for timely progression through G1/S. Cell Prolif *34*, 15–30. 10.1046/j.1365-2184.2001.00192.x.
39. Sidrauski, C., McGeachy, A.M., Ingolia, N.T., and Walter, P. (2015). The small molecule ISRIB reverses the effects of eIF2α phosphorylation on translation and stress granule assembly. eLife *4*, e05033. 10.7554/eLife.05033.
40. Sadighi Akha, A.A., Harper, J.M., Salmon, A.B., Schroeder, B.A., Tyra, H.M., Rutkowski, D.T., and Miller, R.A. (2011). Heightened induction of proapoptotic signals in response to endoplasmic reticulum stress in primary fibroblasts from a mouse model of longevity. J Biol Chem *286*, 30344–30351. 10.1074/jbc.M111.220541.
41. Han, R., Liang, J., and Zhou, B. (2021). Glucose Metabolic Dysfunction in Neurodegenerative Diseases-New Mechanistic Insights and the Potential of Hypoxia as a Prospective Therapy Targeting Metabolic Reprogramming. Int J Mol Sci *22*, 5887. 10.3390/ijms22115887.
42. Wang, L., Shang, Z., Zhou, Y., Hu, X., Chen, Y., Fan, Y., Wei, X., Wu, L., Liang, Q., Zhang, J., et al. (2018). Autophagy mediates glucose starvation-induced glioblastoma cell quiescence and chemoresistance through coordinating cell metabolism, cell cycle, and survival. Cell Death Dis *9*, 213. 10.1038/s41419-017-0242-x.
43. Ryou, M.-G., and Mallet, R.T. (2018). An In Vitro Oxygen-Glucose Deprivation Model for Studying Ischemia-Reperfusion Injury of Neuronal Cells. Methods Mol Biol *1717*, 229–235. 10.1007/978-1-4939-7526-6_18.
44. Shin, S., Buel, G.R., Wolgamott, L., Plas, D.R., Asara, J.M., Blenis, J., and Yoon, S.-O. (2015). ERK2 Mediates Metabolic Stress Response to Regulate Cell Fate. Mol Cell *59*, 382–398. 10.1016/j.molcel.2015.06.020.
45. Oyadomari, S., and Mori, M. (2004). Roles of CHOP/GADD153 in endoplasmic reticulum stress. Cell Death Differ *11*, 381–389. 10.1038/sj.cdd.4401373.
46. Hara, H., Kamiya, T., and Adachi, T. (2011). Endoplasmic reticulum stress inducers provide protection against 6-hydroxydopamine-induced cytotoxicity. Neurochem Int *58*, 35–43. 10.1016/j.neuint.2010.10.006.
47. Huber, A.-L., Lebeau, J., Guillaumot, P., Pétrilli, V., Malek, M., Chilloux, J., Fauvet, F., Payen, L., Kfoury, A., Renno, T., et al. (2013). p58(IPK)-mediated attenuation of the proapoptotic PERK-CHOP pathway allows malignant progression upon low glucose. Mol Cell *49*, 1049–1059. 10.1016/j.molcel.2013.01.009.
48. Park, J.S., Burckhardt, C.J., Lazcano, R., Solis, L.M., Isogai, T., Li, L., Chen, C.S., Gao, B., Minna, J.D., Bachoo, R., et al. (2020). Mechanical regulation of glycolysis via cytoskeleton architecture. Nature *578*, 621–626. 10.1038/s41586-020-1998-1.
49. Travaglini, K.J., Nabhan, A.N., Penland, L., Sinha, R., Gillich, A., Sit, R.V., Chang, S., Conley, S.D., Mori, Y., Seita, J., et al. (2020). A molecular cell atlas of the human lung from single-cell RNA sequencing. Nature *587*, 619–625. 10.1038/s41586-020-2922-4.
50. Kraning-Rush, C.M., and Reinhart-King, C.A. (2012). Controlling matrix stiffness and topography for the study of tumor cell migration. Cell Adhesion & Migration *6*, 274–279. 10.4161/cam.21076.
51. Cameron, H.A. (2006). Quantitative analysis of in vivo cell proliferation. Curr Protoc Neurosci *Chapter 3*, Unit 3.9. 10.1002/N0471142301.ns0309s37.
52. Banerjee, E.R., and Henderson, W.R. (2012). Characterization of lung stem cell niches in a mouse model of bleomycin-induced fibrosis. Stem Cell Res Ther *3*, 21. 10.1186/scrt112.

53. Jia, Y., You, X., Ma, N., Li, H., Liu, G., Wang, Y., Xue, J., Shi, J., Wei, J., Li, Y., et al. (2019). Phenotypic Analysis of BrdU Label-Retaining Cells during the Maturation of Conducting Airway Epithelium in a Porcine Lung. Stem Cells Int *2019*, 7043890. 10.1155/2019/7043890.
54. Wang, Y., Zhang, Z., Chi, Y., Zhang, Q., Xu, F., Yang, Z., Meng, L., Yang, S., Yan, S., Mao, A., et al. (2013). Long-term cultured mesenchymal stem cells frequently develop genomic mutations but do not undergo malignant transformation. Cell Death Dis *4*, e950. 10.1038/cddis.2013.480.
55. Friend, K., Brooks, H.A., Propson, N.E., Thomson, J.A., and Kimble, J. (2015). Embryonic Stem Cell Growth Factors Regulate eIF2α Phosphorylation. PLoS One *10*, e0139076. 10.1371/journal.pone.0139076.
56. Simic, M.S., Moehle, E.A., Schinzel, R.T., Lorbeer, F.K., Halloran, J.J., Heydari, K., Sanchez, M., Jullié, D., Hockemeyer, D., and Dillin, A. (2019). Transient activation of the UPRER is an essential step in the acquisition of pluripotency during reprogramming. Sci Adv *5*, eaaw0025. 10.1126/sciadv.aaw0025.
57. Li, C., Wu, B., Li, Y., Chen, J., Ye, Z., Tian, X., Wang, J., Xu, X., Pan, S., Zheng, Y., et al. (2022). Amino acid catabolism regulates hematopoietic stem cell proteostasis via a GCN2-eIF2α axis. Cell Stem Cell *29*, 1119-1134.e7. 10.1016/j.stem.2022.06.004.
58. Zismanov, V., Chichkov, V., Colangelo, V., Jamet, S., Wang, S., Syme, A., Koromilas, A.E., and Crist, C. (2016). Phosphorylation of eIF2α Is a Translational Control Mechanism Regulating Muscle Stem Cell Quiescence and Self-Renewal. Cell Stem Cell *18*, 79–90. 10.1016/j.stem.2015.09.020.
59. Schultz, E. (1996). Satellite cell proliferative compartments in growing skeletal muscles. Dev Biol *175*, 84–94. 10.1006/dbio.1996.0097.
60. Nair-Gill, E., Bonora, M., Zhong, X., Liu, A., Miranda, A., Stewart, N., Ludwig, S., Russell, J., Gallagher, T., Pinton, P., et al. (2021). Calcium flux control by Pacs1-Wdr37 promotes lymphocyte quiescence and lymphoproliferative diseases. EMBO J *40*. 10.15252/embj.2020104888.
61. Xin, Y., Malick, A., Hu, M., Liu, C., Batah, H., Xu, H., and Duan, C. (2019). Cell-autonomous regulation of epithelial cell quiescence by calcium channel Trpv6. eLife *8*, e48003. 10.7554/eLife.48003.
62. van Vliet, A.R., Giordano, F., Gerlo, S., Segura, I., Van Eygen, S., Molenberghs, G., Rocha, S., Houcine, A., Derua, R., Verfaillie, T., et al. (2017). The ER Stress Sensor PERK Coordinates ER-Plasma Membrane Contact Site Formation through Interaction with Filamin-A and F-Actin Remodeling. Mol Cell *65*, 885-899.e6. 10.1016/j.molcel.2017.01.020.
63. Urra, H., Henriquez, D.R., Cánovas, J., Villarroel-Campos, D., Carreras-Sureda, A., Pulgar, E., Molina, E., Hazari, Y.M., Limia, C.M., Alvarez-Rojas, S., et al. (2018). IRE1α governs cytoskeleton remodelling and cell migration through a direct interaction with filamin A. Nat Cell Biol *20*, 942–953. 10.1038/s41556-018-0141-0.
64. Secondo, A., Petrozziello, T., Tedeschi, V., Boscia, F., Vinciguerra, A., Ciccone, R., Pannaccione, A., Molinaro, P., Pignataro, G., and Annunziato, L. (2019). ORAI1/STIM1 Interaction Intervenes in Stroke and in Neuroprotection Induced by Ischemic Preconditioning Through Store-Operated Calcium Entry. Stroke *50*, 1240–1249. 10.1161/STROKEAHA.118.024115.
65. Hooper, R., Zhang, X., Webster, M., Go, C., Kedra, J., Marchbank, K., Gill, D.L., Weeraratna, A.T., Trebak, M., and Soboloff, J. (2015). Novel Protein Kinase C-Mediated Control of Orai1 Function in Invasive Melanoma. Mol Cell Biol *35*, 2790–2798. 10.1128/MCB.01500-14.
66. Mekahli, D., Bultynck, G., Parys, J.B., De Smedt, H., and Missiaen, L. (2011). Endoplasmic-reticulum calcium depletion and disease. Cold Spring Harb Perspect Biol *3*, a004317. 10.1101/cshperspect.a004317.
67. Pinton, P., Giorgi, C., Siviero, R., Zecchini, E., and Rizzuto, R. (2008). Calcium and apoptosis: ER-mitochondria Ca2+ transfer in the control of apoptosis. Oncogene *27*, 6407–6418. 10.1038/onc.2008.308.
68. Han, S.J., Kwon, S., and Kim, K.S. (2021). Challenges of applying multicellular tumor spheroids in preclinical phase. Cancer Cell Int *21*, 152. 10.1186/s12935-021-01853-8.

69. Cantor, J.R., Abu-Remaileh, M., Kanarek, N., Freinkman, E., Gao, X., Louissaint, A., Lewis, C.A., and Sabatini, D.M. (2017). Physiologic Medium Rewires Cellular Metabolism and Reveals Uric Acid as an Endogenous Inhibitor of UMP Synthase. Cell *169*, 258-272.e17. 10.1016/j.cell.2017.03.023.
70. Vande Voorde, J., Ackermann, T., Pfetzer, N., Sumpton, D., Mackay, G., Kalna, G., Nixon, C., Blyth, K., Gottlieb, E., and Tardito, S. (2019). Improving the metabolic fidelity of cancer models with a physiological cell culture medium. Sci. Adv. *5*, eaau7314. 10.1126/sciadv.aau7314.
71. Paiva, S., Joanne, P., Migdal, C., Soler, E.L., Hovhannisyan, Y., Nicolas, A., and Agbulut, O. (2020). Polyacrylamide Hydrogels with Rigidity-Independent Surface Chemistry Show Limited Long-Term Maintenance of Pluripotency of Human Induced Pluripotent Stem Cells on Soft Substrates. ACS Biomater. Sci. Eng. *6*, 340–351. 10.1021/acsbiomaterials.9b01189.
72. Tajan, M., Hock, A.K., Blagih, J., Robertson, N.A., Labuschagne, C.F., Kruiswijk, F., Humpton, T.J., Adams, P.D., and Vousden, K.H. (2018). A Role for p53 in the Adaptation to Glutamine Starvation through the Expression of SLC1A3. Cell Metab *28*, 721-736.e6. 10.1016/j.cmet.2018.07.005.
73. Schmidt, E.K., Clavarino, G., Ceppi, M., and Pierre, P. (2009). SUnSET, a nonradioactive method to monitor protein synthesis. Nat Methods *6*, 275–277. 10.1038/nmeth.1314.
74. Bouizakarne, S., Etienne, J., and Nicolas, A. (2023). Impact of baculoviral transduction of fluorescent actin on cellular forces. European Journal of Cell Biology *102*, 151294. 10.1016/j.ejcb.2023.151294.
75. Galaxy Community (2022). The Galaxy platform for accessible, reproducible and collaborative biomedical analyses: 2022 update. Nucleic Acids Res *50*, W345-351. 10.1093/nar/gkac247.
76. Zhou, G., Soufan, O., Ewald, J., Hancock, R.E.W., Basu, N., and Xia, J. (2019). NetworkAnalyst 3.0: a visual analytics platform for comprehensive gene expression profiling and meta-analysis. Nucleic Acids Res *47*, W234–W241. 10.1093/nar/gkz240.
77. Hao, Y., Hao, S., Andersen-Nissen, E., Mauck, W.M., Zheng, S., Butler, A., Lee, M.J., Wilk, A.J., Darby, C., Zager, M., et al. (2021). Integrated analysis of multimodal single-cell data. Cell *184*, 3573-3587.e29. 10.1016/j.cell.2021.04.048.
78. Stuart, T., Butler, A., Hoffman, P., Hafemeister, C., Papalexi, E., Mauck, W.M., Hao, Y., Stoeckius, M., Smibert, P., and Satija, R. (2019). Comprehensive Integration of Single-Cell Data. Cell *177*, 1888-1902.e21. 10.1016/j.cell.2019.05.031.
79. Wolf, F.A., Angerer, P., and Theis, F.J. (2018). SCANPY: large-scale single-cell gene expression data analysis. Genome Biol *19*, 15. 10.1186/s13059-017-1382-0.
80. Chen, E.Y., Tan, C.M., Kou, Y., Duan, Q., Wang, Z., Meirelles, G.V., Clark, N.R., and Ma'ayan, A. (2013). Enrichr: interactive and collaborative HTML5 gene list enrichment analysis tool. BMC Bioinformatics *14*, 128. 10.1186/1471-2105-14-128.
81. Kuleshov, M.V., Jones, M.R., Rouillard, A.D., Fernandez, N.F., Duan, Q., Wang, Z., Koplev, S., Jenkins, S.L., Jagodnik, K.M., Lachmann, A., et al. (2016). Enrichr: a comprehensive gene set enrichment analysis web server 2016 update. Nucleic Acids Res *44*, W90-97. 10.1093/nar/gkw377.
82. Pont, F., Tosolini, M., and Fournié, J.J. (2019). Single-Cell Signature Explorer for comprehensive visualization of single cell signatures across scRNA-seq datasets. Nucleic Acids Research *47*, e133–e133. 10.1093/nar/gkz601.

Figure 1

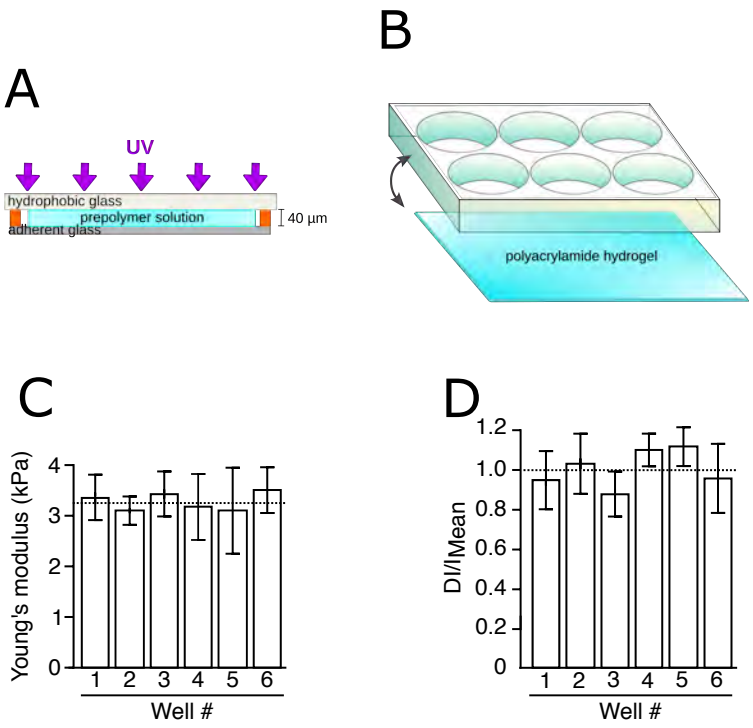

Figure 2

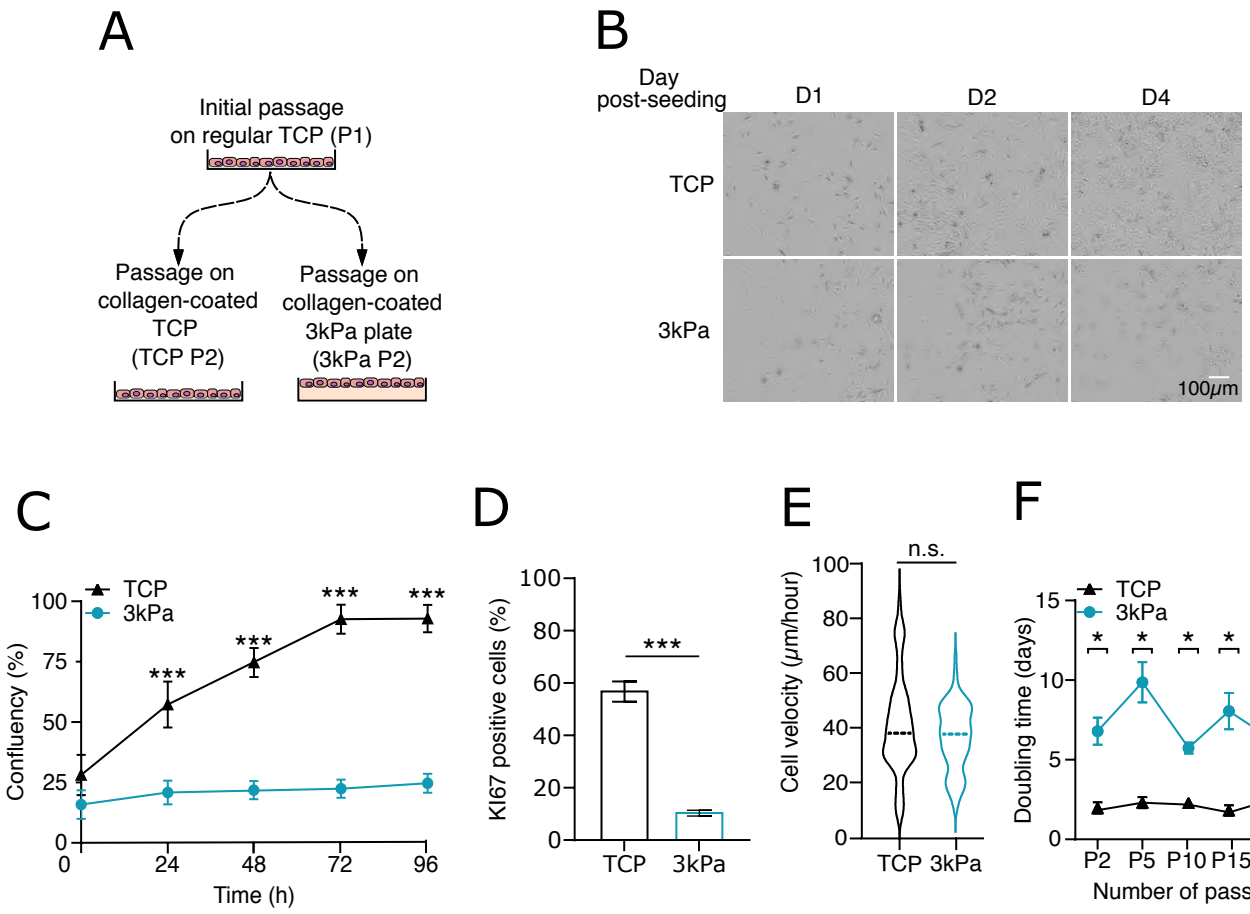

Figure 3

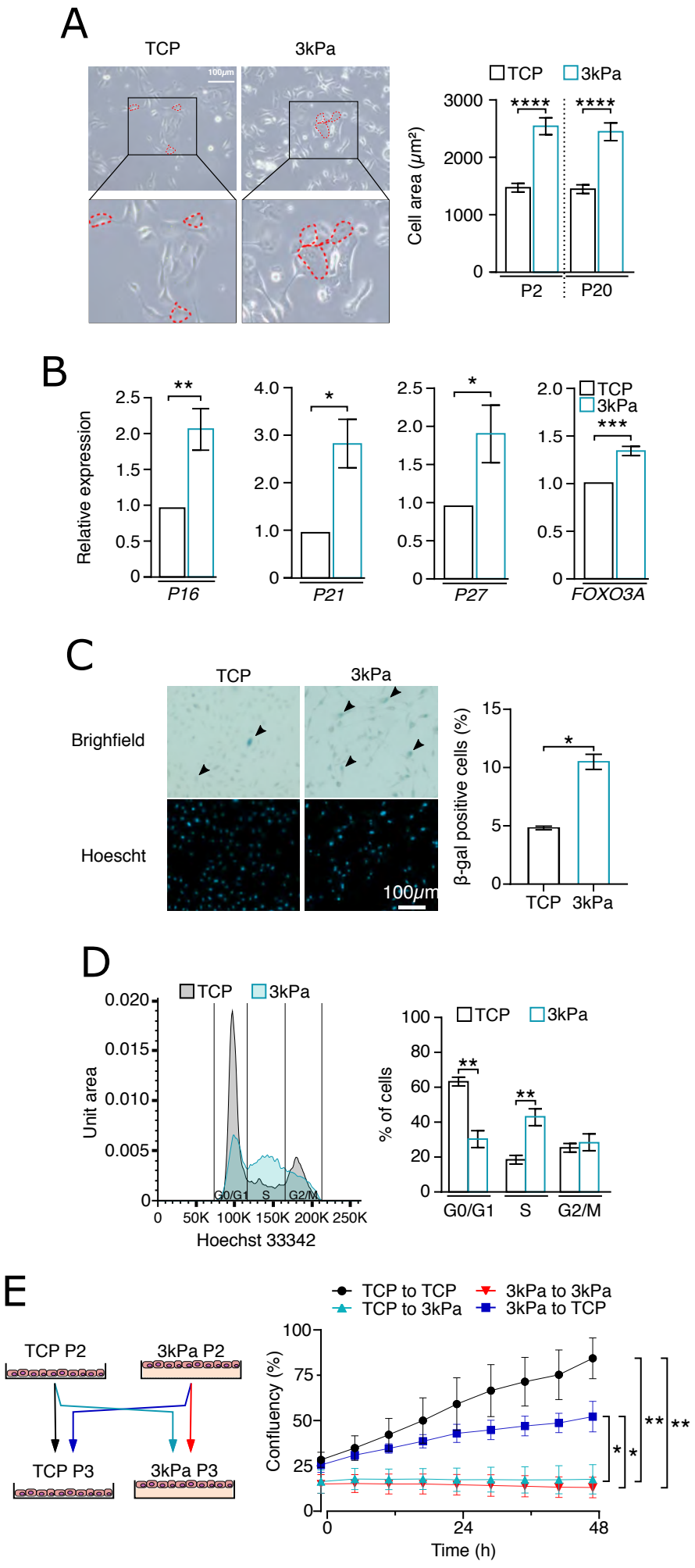

Figure 4

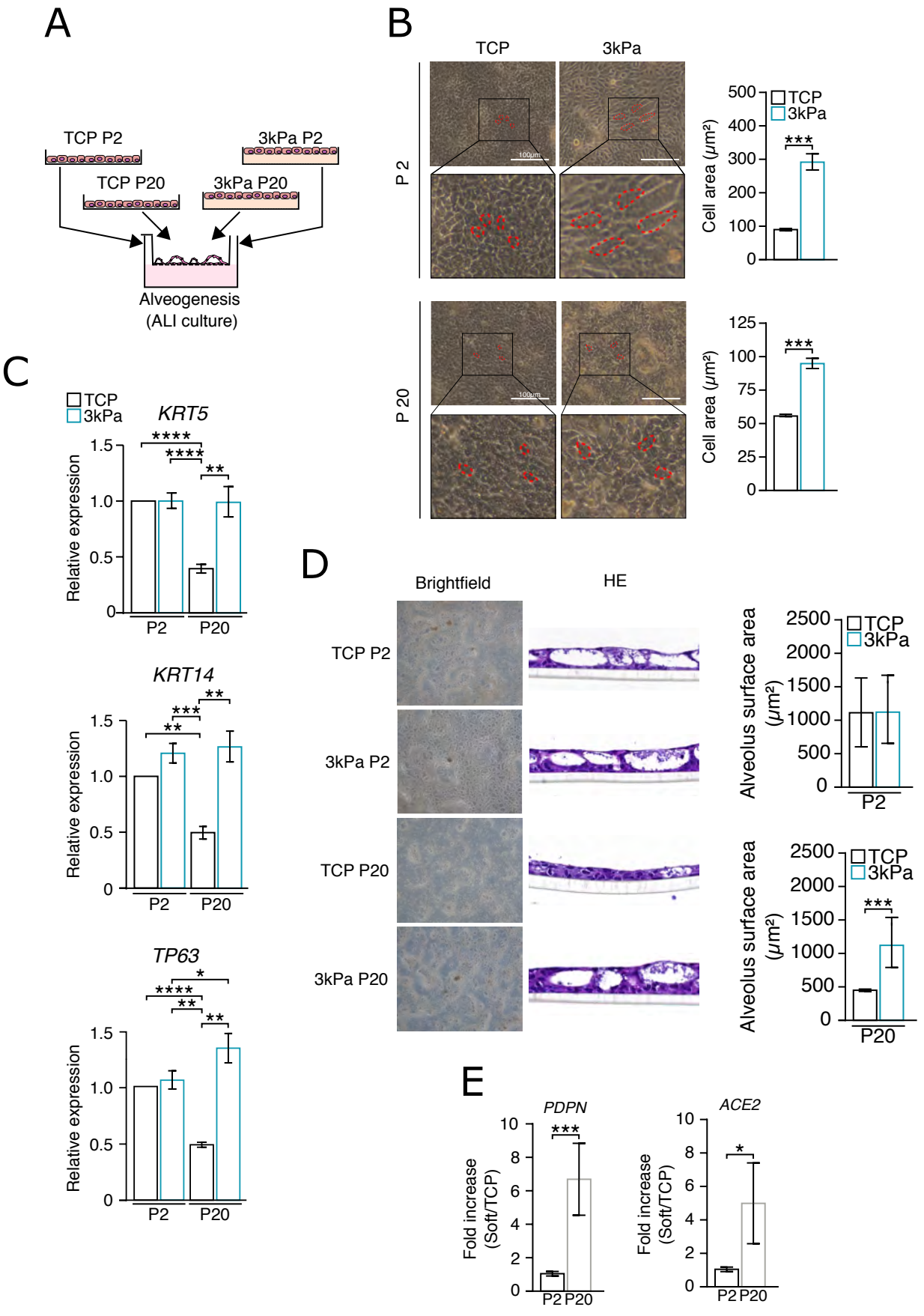

Figure 5

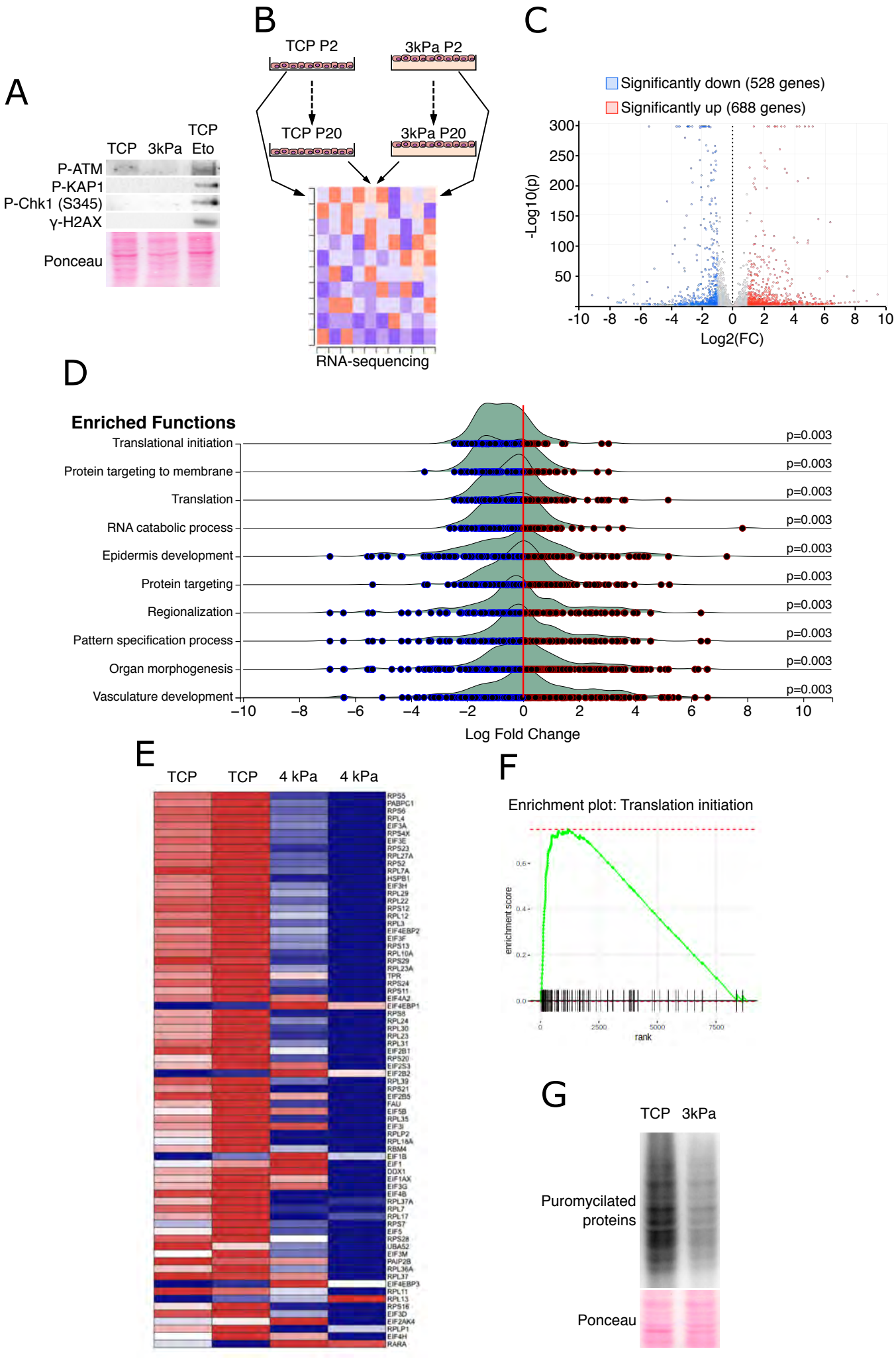

Figure 6

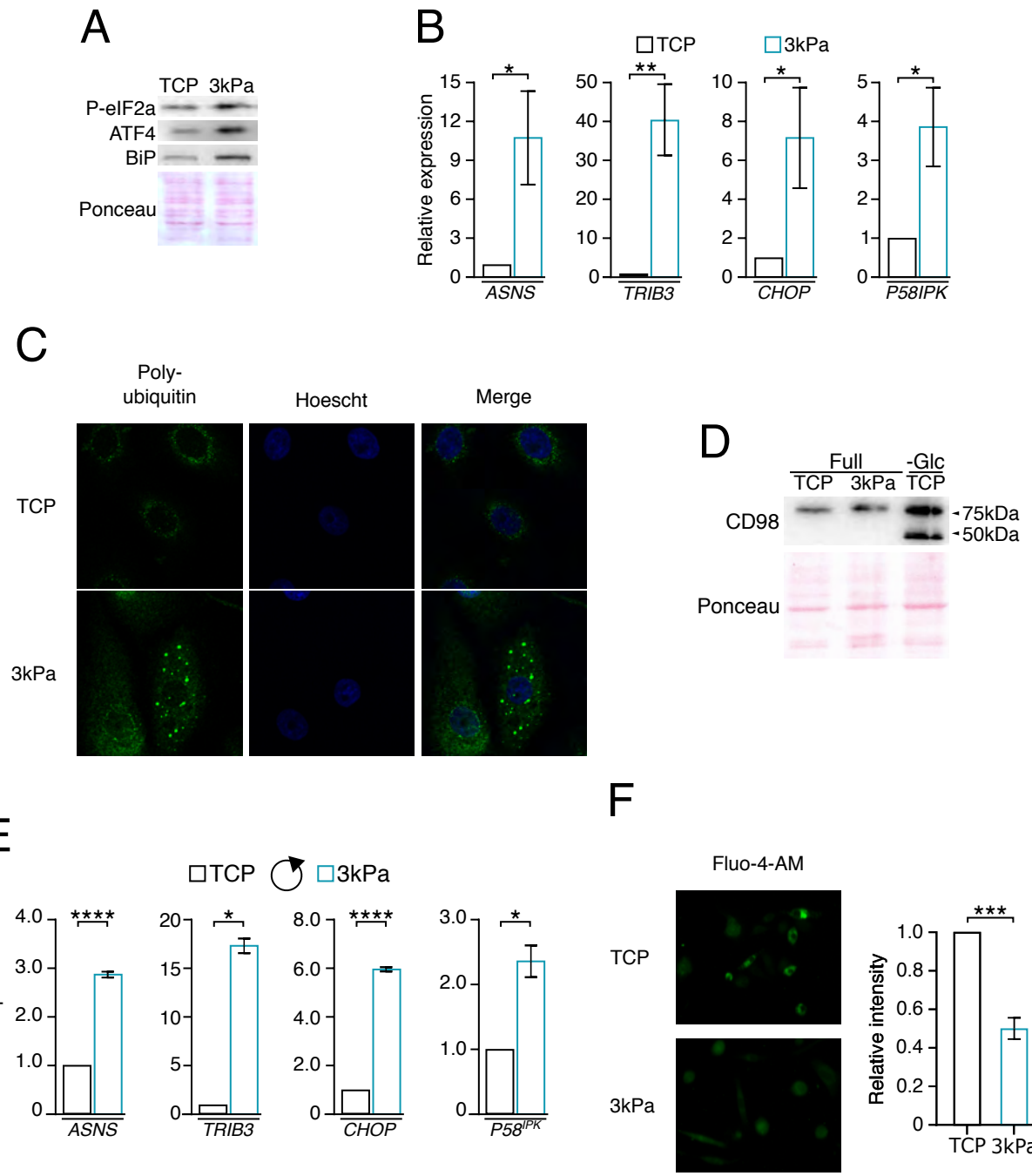

Figure 7

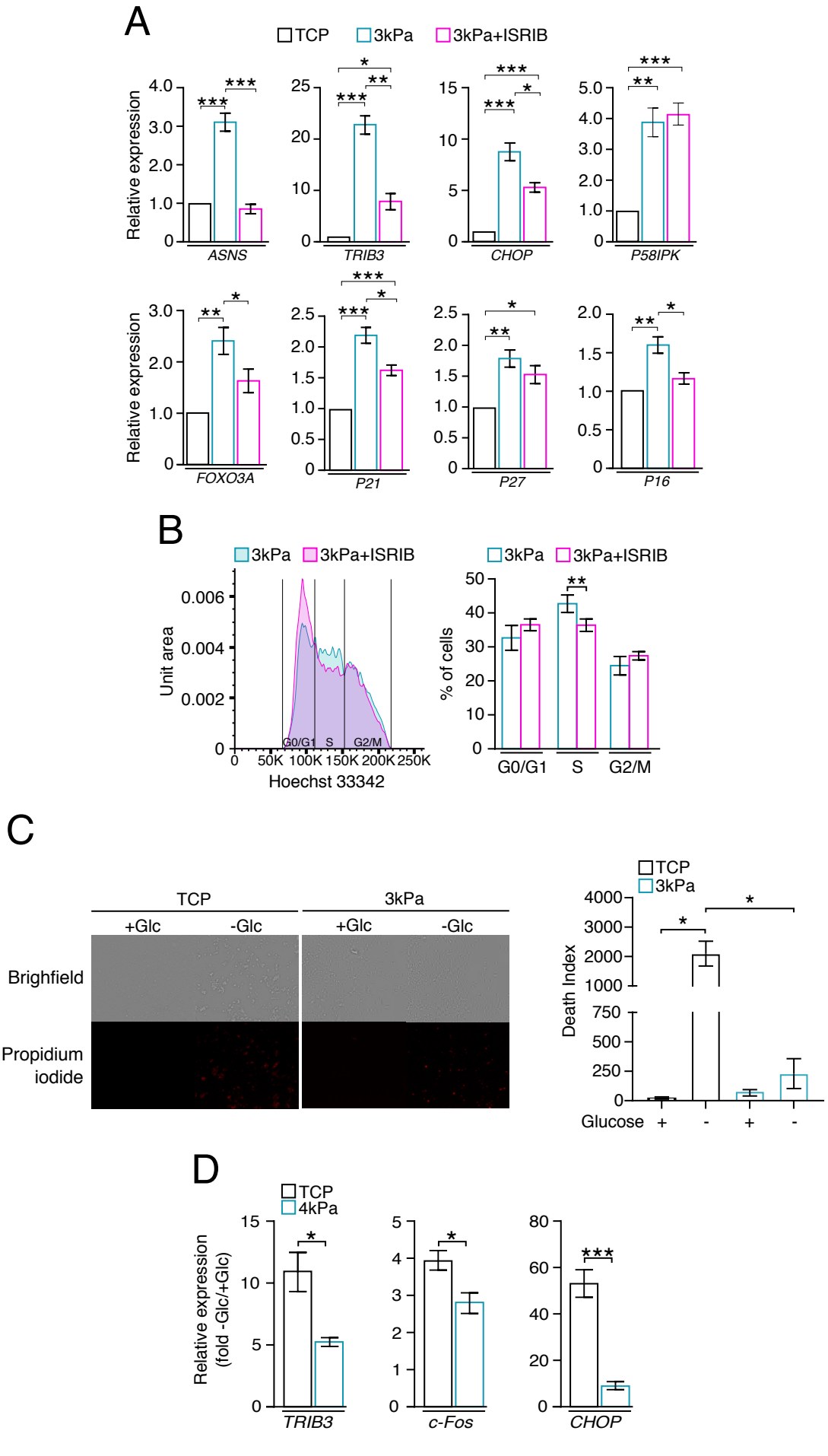

Figure 8